AMERICAN SOCIETY FOR MICROBIOLOGY | Journal of Virology

Immunology | Full-Length Text

The frequency and function of nucleoprotein-specific CD8$^+$ T cells are critical for heterosubtypic immunity against influenza virus infection

Samuel Amoah,[1] Weiping Cao,[1] Ekramy E. Sayedahmed,[2] Yuanyuan Wang,[3] Amrita Kumar,[1] Margarita Mishina,[1] Devon J. Eddins,[1] Wen-Chien Wang,[2] Mark Burroughs,[3] Mili Sheth,[3] Justin Lee,[3] Wun-Ju Shieh,[4] Sean D. Ray,[5] Caitlin D. Bohannon,[1] Priya Ranjan,[1] Suresh D. Sharma,[1] Jessica Hoehner,[6] Robert A. Arthur,[6] Shivaprakash Gangappa,[1] Nobuko Wakamatsu,[7] H. Richard Johnston,[8] Jan Pohl,[3] Suresh K. Mittal,[2] Suryaprakash Sambhara[1]

AUTHOR AFFILIATIONS See affiliation list on p. 17.

ABSTRACT Cytotoxic T lymphocytes (CTLs) mediate host defense against viral and intracellular bacterial infections and tumors. However, the magnitude of CTL response and their function needed to confer heterosubtypic immunity against influenza virus infection are unknown. We addressed the role of CD8$^+$ T cells in the absence of any cross-reactive antibody responses to influenza viral proteins using an adenoviral vector expressing a 9mer amino acid sequence recognized by CD8$^+$ T cells. Our results indicate that both CD8$^+$ T cell frequency and function are crucial for heterosubtypic immunity. Low morbidity, lower viral lung titers, low to minimal lung pathology, and better survival upon heterosubtypic virus challenge correlated with the increased frequency of NP-specific CTLs. NP-CD8$^+$ T cells induced by differential infection doses displayed distinct RNA transcriptome profiles and functional properties. CD8$^+$ T cells induced by a high dose of influenza virus secreted significantly higher levels of IFN-γ and exhibited higher levels of cytotoxic function. The mice that received NP-CD8$^+$ T cells from the high-dose virus recipients through adoptive transfer had lower viral titers following viral challenge than those induced by the low dose of virus, suggesting differential cellular programming by antigen dose. Enhanced NP-CD8$^+$ T-cell functions induced by a higher dose of influenza virus strongly correlated with the increased expression of cellular and metabolic genes, indicating a shift to a more glycolytic metabolic phenotype. These findings have implications for developing effective T cell vaccines against infectious diseases and cancer.

IMPORTANCE Cytotoxic T lymphocytes (CTLs) are an important component of the adaptive immune system that clears virus-infected cells or tumor cells. Hence, developing next-generation vaccines that induce or recall CTL responses against cancer and infectious diseases is crucial. However, it is not clear if the frequency, function, or both are essential in conferring protection, as in the case of influenza. In this study, we demonstrate that both CTL frequency and function are crucial for providing heterosubtypic immunity to influenza by utilizing an Ad-viral vector expressing a CD8 epitope only to rule out the role of antibodies, single-cell RNA-seq analysis, as well as adoptive transfer experiments. Our findings have implications for developing T cell vaccines against infectious diseases and cancer.

KEYWORDS influenza, CTL, adeno vector, RNA-seq

With an estimated 12,000–61,000 people dying annually from infection in the United States, the influenza virus continues to be a pathogen of importance

Editor Paul G. Thomas, St. Jude Children's Research Hospital, Memphis, Tennessee, USA

Address correspondence to Suryaprakash Sambhara, ssambhara@cdc.gov, or Suresh K. Mittal, mittal@purdue.edu.

Samuel Amoah, Weiping Cao, and Ekramy E. Sayedahmed contributed equally to this article. Author order was determined both alphabetically and in order of concept development, experimental contribution, and reagent developoment.

The authors declare no conflict of interest.

See the funding table on p. 18.

Received 24 April 2024
Accepted 27 June 2024
Published 31 July 2024

despite being a vaccine-preventable infectious disease (1). Vaccine-induced antibody responses primarily target the head region of hemagglutinin (HA), which blocks virus attachment to hosts' cell surfaces and prevents infection (2, 3). However, due to the lack of proofreading mechanisms of the virally encoded RNA-dependent RNA polymerases, frequent mutations occur during influenza virus genome replication leading to antigenic drift (4). Because antibodies induced against the major virus surface protein, HA, tend to be strain-specific, vaccines must be updated annually to match the circulating strains (5). Cytotoxic T lymphocytes (CTLs) recognize highly conserved viral proteins and play a significant role in heterosubtypic immunity across influenza strains (6–9). $CD8^+$ CTLs against the polymerase-binding protein (PB1), matrix 1 (M1), and nucleoprotein (NP) play an essential role in immune responses against influenza virus infection (10–12). Recent studies during the 2009 pandemic with H1N1 virus demonstrated that individuals with higher frequencies of preexisting cross-reactive CTLs had milder symptoms and a lower risk of virus shedding (13). In addition, a study using low- and high-avidity CTL lines induced with a recombinant vaccinia virus expressing HIV-GP16 and stimulated *in vitro* with different concentrations of peptides suggests that the quality of CTLs is as important as the quantity of CTLs (14). However, the role of CTL frequency and quality for heterosubtypic protection against influenza virus infection remains unclear.

CTL responses against influenza virus infection in C57Bl/6 mice include H-$2D^b$-restricted $NP_{366–374}$, $D^bPA_{224–233}$, $D^bPB1\text{-}F2_{62–70}$, $K^bPB1_{703–711}$, $K^bNS2_{114–121}$, and $K^bM1_{128–135}$. However, $NP_{366\text{-}374}$ is abundant and CTL responses against NP are also dominant post-infection, while responses to other epitopes are subdominant. Hence, we addressed $CD8^+$ T cell responses against the dominant epitope $NP_{366\text{-}374}$. In this study, using a mouse model with an H1N1 (PR8 virus) primary infection followed by an H3N2 (HK68 virus) challenge, we demonstrated that the increased frequency of NP-$CD8^+$ T cells is essential for heterosubtypic protection without causing significant lung pathology. We further confirmed this finding using an adenoviral vector expressing the H1N1 NP $CD8^+$ T cell epitope (HAd-NPCD8) in the absence of any NP-specific antibody response. Results showed that a high frequency of NP-specific $CD8^+$ T cells correlated with increased survival after heterosubtypic challenge with the HK68 virus in the absence of antibodies against NP. In addition, NP-$CD8^+$ T cells induced by different virus doses displayed differential transcriptional reprogramming profiles and are different in cellular and metabolic profiles. Furthermore, CD8+ T cells induced by the higher virus dose secreted higher levels of IFN-γ, exhibited higher levels of cytotoxic function, and reduced viral titer following viral challenge on adoptive transfer. Therefore, the quantity and function of NP-$CD8^+$ T cells are both essential in heterosubtypic immunity against influenza virus infection.

RESULTS

The frequency of NP-specific $CD8^+$ T cells induced is proportional to the infectious dose

Mice were inoculated with increasing doses [2, 10, and 20 50% mouse infectious dose (MID_{50})] of PR8 (H1N1) influenza virus and monitored for body weight changes. Mice infected with the highest dose, 20 MID_{50}, displayed morbidity between days 6 and 11 post-infection compared to the naive group (Fig. 1A). The duration of morbidity was shorter for mice infected with the 10 MID_{50} PR8 virus occurring from day 7 to 10 post-infection. No differences were observed in body weight change between the 2 MID_{50} infection dose and the naive group (Fig. 1A). We examined the frequency of NP-specific $CD8^+$ T cells 4 weeks post-infection using flow cytometry with $NP_{366\text{-}374}$-H-$2D^b$ tetramers in conjunction with antibodies specific for CD8 and the activation marker CD44. The HK68-specific response allowed us to examine the cross-reactive T cell pool size before the heterosubtypic challenge. HK68 epitope has D and A at P7 and P8 positions, while PR8 has E and T at P7 and P8 positions, respectively; however, PR8 NP-reactive cells could cross-react with HK68 NP tetramers. Mice immunized with

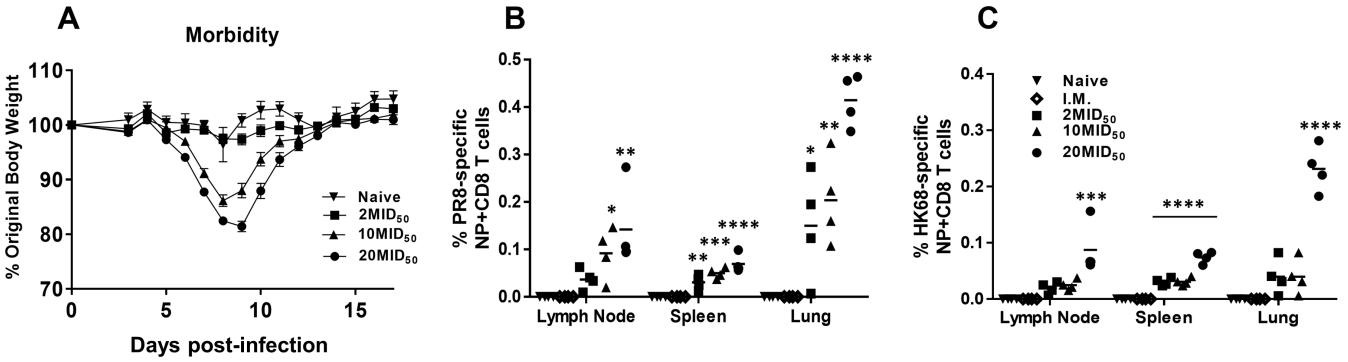

FIG 1 The frequency of NP-specific CD8$^+$ T cells induced is proportional to the influenza virus dose. Six-week-old female C57BL/6 mice (Jackson Laboratory, Bar Harbor, ME, USA) were anesthetized by inhalation of isoflurane and infected intranasally with 2, 10, and 20 MID_{50} of PR8 virus in a final volume of 50 µL. Control mice were either given PBS or immunized with a dose of 500 hemagglutinin units in 50 µL of formalin-inactivated PR8 virus in each quadriceps muscle. (A) The mice were monitored for body weight changes up to 17 days post-PR8 virus infection. Data are an aggregate of 38 mice per group from three independent experiments for the infected groups and four for the naive group (two independent experiments). (B and C) Four weeks post-infection, the draining lymph nodes, spleen, and lung tissues were harvested, and single-cell suspensions were prepared. Activated CD8$^+$ T cells in the tissues were identified using anti-CD8 and anti-CD44 antibodies. PR8 (B) or HK68 (C) virus NP-specific CD8$^+$ T cells in the tissues were identified using H-2D^b/ASNENMETM or H-2D^b/ ASNENMDAM tetramers, respectively. Data are from two independent experiments with at least four mice per group. One-way ANOVA with multiple comparisons was used to analyze the differences between treated and naive control groups. *P < 0.05, **P < 0.01, ***P < 0.001, and ****P < 0.0001 compared to the naive control group.

formalin-inactivated (FI) PR8 virus intramuscularly (I.M.) induced little-to-no CD8$^+$ T cell responses (Fig. 1B and C). NP-specific CD8$^+$ T cell responses showed dose-dependent increases, and mice infected with the highest dose of the virus, the 20 MID_{50}, had the highest frequency of NP-CD8$^+$ T cells in all tissues examined (Fig. 1B). Especially in the lungs, PR8 virus-infected mice displayed a significantly higher frequency of antigen-specific CD8+ T cells than the naive or I.M. immunized group (Fig. 1B). The HK68-specific response demonstrated a similar trend as the PR8-specific response. Furthermore, in all three tissues examined (spleen, lymph node, and lung), mice infected with the 20 MID_{50} infectious dose had a statistically significant increase of antigen-specific T cells as compared to the naive or I.M. immunized group (Fig. 1C). Thus, the frequency of reactive and cross-reactive NP-specific CD8$^+$ T cells induced is proportional to the virus dose. All three groups had various levels of detectable NP-specific CD8$^+$ T cells post-primary infection, as demonstrated in Fig. 1. NP 366–374 epitope for D^b is well conserved among several influenza viruses, and their sequence homology is shown in Fig. 2. D^b allele-specific anchor residues warrant peptides to have "S" at position 2, "N" at position 5 and "M," "I," "L," or "V" at position 9 (15–17). In addition, P3 can serve as a secondary anchor position. P4, P6, P7, and P8 serve as TCR contact residues. Both the PR8- and HK68-specific NP CD8$^+$ T cells were detected in the lymph node, spleen, and lung tissues.

Morbidity and survival are proportional to NP-specific CD8$^+$ T cell frequency on the heterosubtypic challenge

Mice immunized with different doses of PR8 (H1N1) influenza virus were challenged with 2 LD_{50} of HK68 (H3N2) influenza virus and monitored for morbidity, survival, lung histopathology, serological responses against PR8 and HK/68, and lung viral titers. As shown in Fig. 3A and B, mice that received the high infectious doses (20 MID_{50} and 10 MID_{50}) of PR8 lost the least body weight, and all mice survived upon heterosubtypic challenge. Mice infected with 2 MID_{50} of the PR8 virus had moderate weight loss, and 90% of those mice survived the challenge. However, groups of mice with no NP-specific CD8$^+$ T cell response, the naive and I.M. group, succumbed to the challenge by day 6 (Fig. 3B). We also examined the lung pathology on day 5 post-HK68 virus challenge using hematoxylin and eosin (H&E) staining of lung sections (Fig. 3C). Naive mice without viral challenge did not contain any inflammatory cells (score = 0). However, mice with HK/68 challenge had moderate peribronchiolar and alveolar inflammation (score = 2).

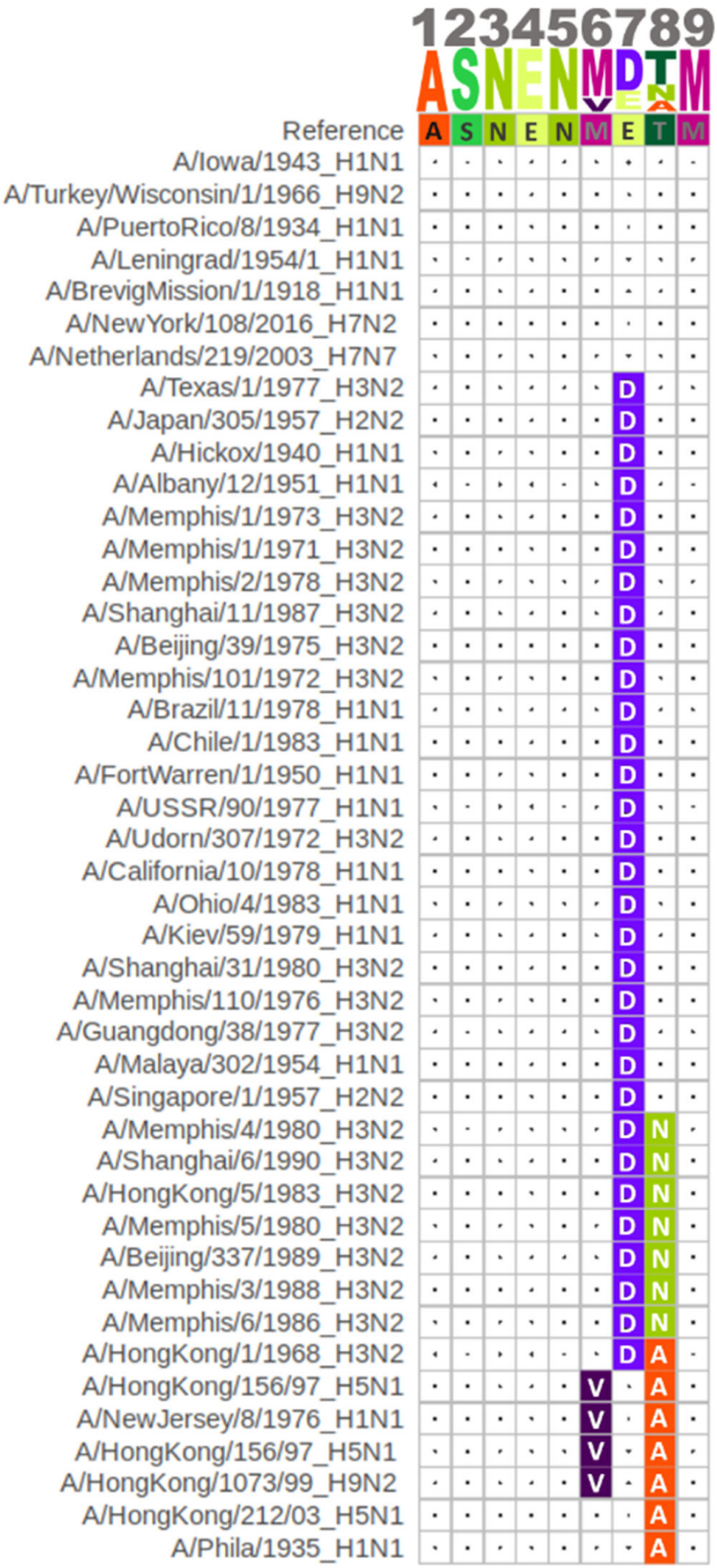

FIG 2 Sequence homology of NP across different influenza viruses. P2, P5, and P9 serve as primary anchors for D^b allele-specific binding with a requirement for "S" at position 2, "N" at position 5, and "M," "I," "L," or "V" at position 9. In addition, P3 can serve as a secondary anchor position. P4, P6, P7, and P8 serve as TCR contact residues.

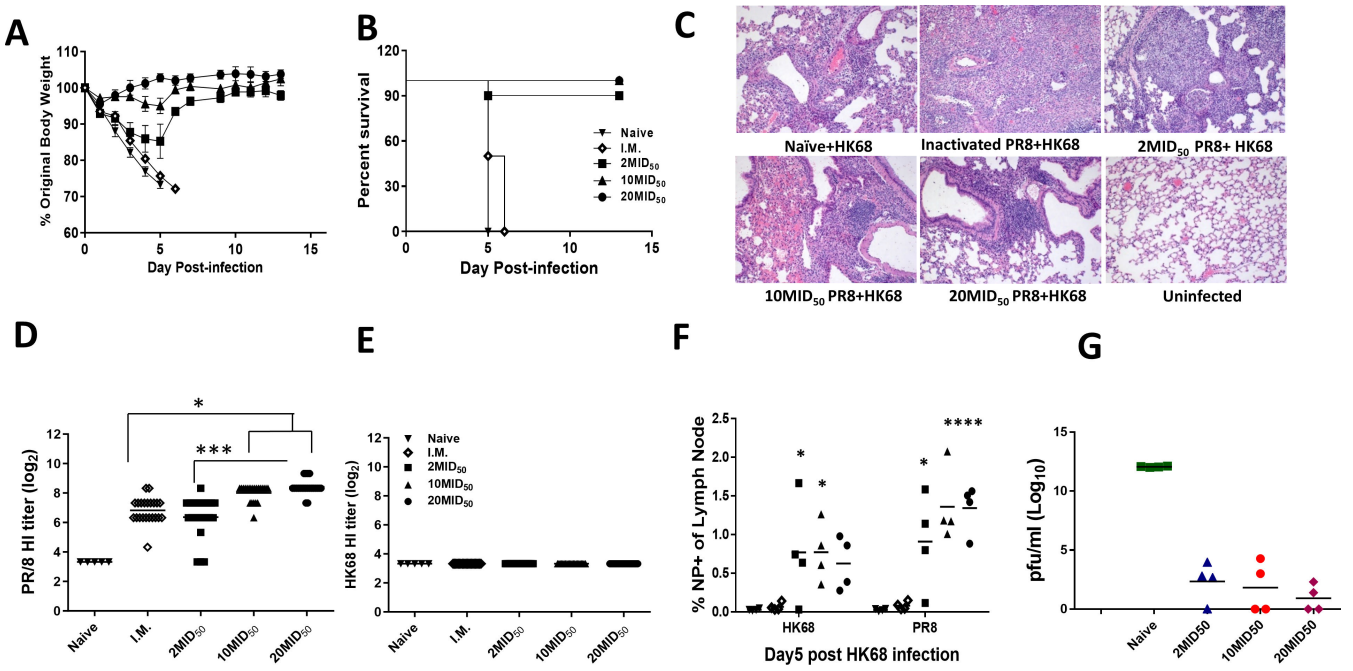

FIG 3 Increased NP-specific CD8$^+$ T cell frequency correlates with low morbidity, increased survival, and enhanced viral clearance on a heterosubtypic challenge. Six-week-old female C57BL/6 mice (Jackson Laboratory, Bar Harbor, ME, USA) were anesthetized by inhalation of isoflurane and infected intranasally (I.N.) with 2, 10, and 20 MID_{50} of PR8 virus in a final volume of 50 µL. Control mice received PBS or immunized I.M. with a dose of 500 hemagglutinin units (HAU) in 50 µL of formalin-inactivated PR8 virus in each quadriceps muscle. (A and B) Mice were challenged 4 weeks post-infection with 2 LD_{50} of HK68 (H3N2) influenza virus and monitored for morbidity (A) and mortality (B). Data represented two independent experiments with at least four mice per group. (C) Five days post-heterosubtypic challenge, lungs were harvested and fixed in 10% neutral-buffered formalin. After 72 h, the samples were transferred to 70% ethanol, sectioned, and stained with hematoxylin and eosin. (D and E) Six-week-old female C57BL/6 mice (Jackson Laboratory, Bar Harbor, ME, USA) were anesthetized by inhalation of isoflurane and infected I.N. with 2, 10, and 20 MID_{50} of PR8 virus in a final volume of 50 µL. Control mice received PBS or were immunized with a dose of 500 HAU in 50 µL of formalin-inactivated PR8 virus by I.M. route in each quadriceps muscle. Four weeks post-infection, sera were collected and examined for HI titers to PR8 virus (D) or HK68 virus (E). Data are from 22 mice from two independent experiments for infected or vaccinated groups and 10 from three independent experiments for the naive group. (F) Four weeks post-infection, mice were challenged with 2 LD_{50} of HK68 (H3N2) influenza virus. Lung tissues were harvested, and single-cell suspensions were prepared. Activated CD8$^+$ T cells in the tissues were identified using anti-CD8 and anti-CD44 antibodies. PR8- or HK68-specific NP CD8$^+$ T cells in the tissues were identified using H-2D^b/ASNENMETM or H-2D^b/ ASNENMDAM tetramers, respectively. Data represent two independent experiments with at least four mice per group. One-way ANOVA with multiple comparisons was used to analyze the differences between treatment and naive control groups. *P < 0.05 and ****P < 0.0001 compared to the naive control group. (G) Lungs were also collected to determine viral titers on day 3 post-HK68 challenge, and the study was repeated at least twice with a minimum of four mice per group.

Mice primed with 2, 10, or 20 MID_{50} PR8 and challenged with HK68 had an average inflammation score of 1.

Before the heterosubtypic virus challenge, we measured the HI titers to the PR8 and HK68 viruses to rule out the possibility of cross-reactive antibodies from the PR8-infected or PR8-immunized mice. We observed a dose-dependent increase in HI titers against the PR8 virus (Fig. 3D). Responses were significantly different for the 10 MID_{50} and 20 MID_{50} groups compared to the other groups. Mice infected with 2 MID_{50} of PR8 virus or immunized I.M. with formalin-inactivated PR8 virus had similar levels of antibody titers. Most importantly, there were no cross-reactive HI antibodies against the challenge HK68 virus (Fig. 3E). However, we cannot rule out cross-reactive antibody responses against the stem as the HI test cannot detect them. In addition, on day 5 post-heterosubtypic challenge, the frequency of PR8-specific NP-CD8$^+$ T cells was much higher than the HK68-specific NP-CD8$^+$ T cells (Fig. 3F) in the previously PR/8-infected mice, possibly due to original antigen sin of CD8$^+$ T cells (18). In addition, mice that received the higher infecting doses of the PR8 virus displayed lesser cellular infiltration and more normal lung tissue structure when compared to those that received the lower doses of the virus.

There was a significant reduction in viral titers in all infection dose groups in lungs 5 days post-HK68 viral challenge (P = 0.00390) compared to naive mice challenged with HK68 virus (Fig. 3G). Although there was a dose-dependent reduction in lung viral titers, it was not significant. These data demonstrated that increased frequencies of NP-specific CD8$^+$ T cells result in lower morbidity, enhanced survival, reduced lung pathology, and reduced viral titers following the heterosubtypic virus challenge.

Increased frequency of NP-specific CD8$^+$ T cells is sufficient for enhanced survival after heterosubtypic challenge

To rule out the effect of NP-specific antibodies, we immunized mice with 1 × 10^6, 1 × 10^7, 1 × 10^8, or 1 × 10^9 PFU/mouse of a replication-defective adenovirus with deletions in the E1 and E3 regions expressing the PR8 NP epitope (HAd-NPCD8). We examined the NP-CD8$^+$ T cell responses prior to the heterosubtypic virus challenge. As controls, mice were immunized intranasally (I.N.) with 1 × 10^9 PFU/mouse with the same vector but without any influenza epitopes (HAd-ΔE1E3) or PBS. As shown in Fig. 4A, there was a dose-dependent increase in the number of NP-CD8$^+$ T cells in the lungs. Mice receiving 1

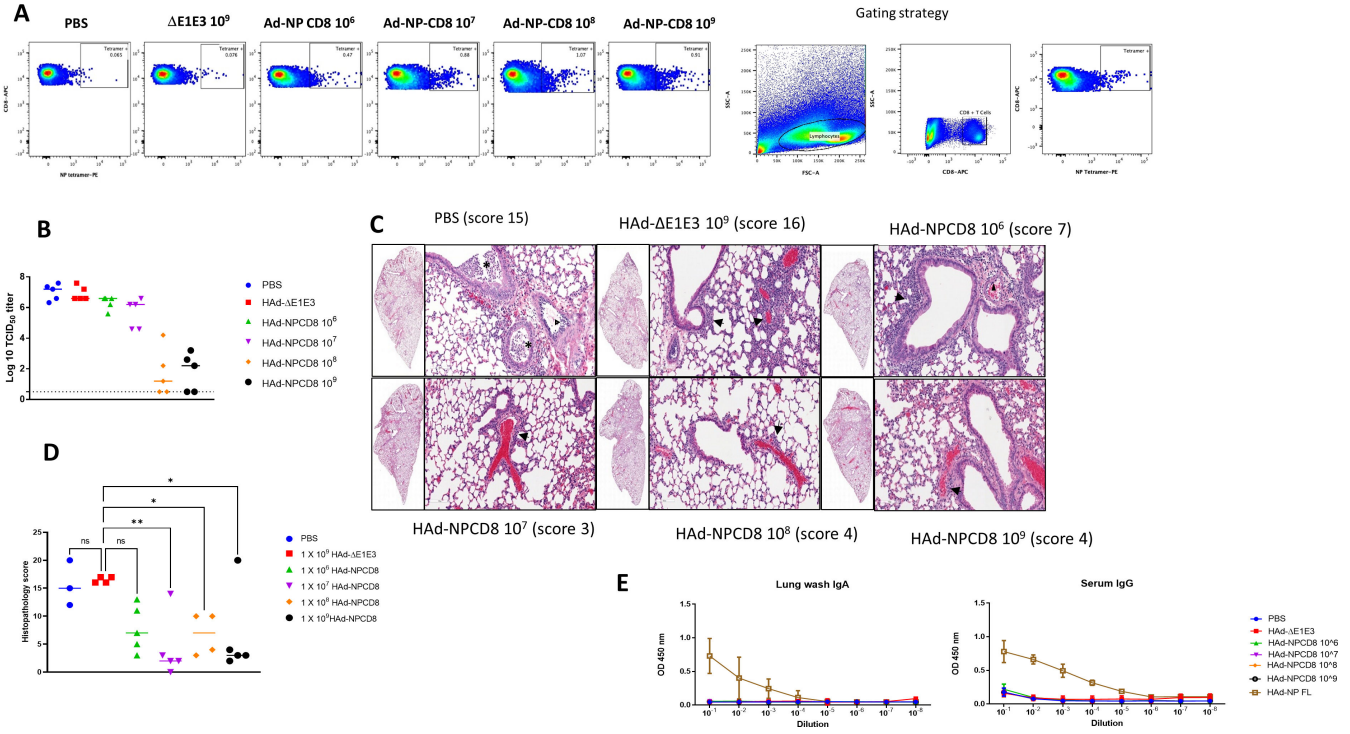

FIG 4 Increased frequency of NP-specific CD8$^+$ T cells is sufficient for improved survival after heterosubtypic challenge. Six-week-old female C57BL/6 mice (Jackson Laboratory, Bar Harbor, ME, USA) were anesthetized and inoculated I.N. with 1 × 10^6, 1 × 10^7, 1 × 10^8, and 1 × 10^9 PFU/mouse HAd-NPCD8 or 1 × 10^9 PFU/mouse HAd-ΔE1E3. Control mice were inoculated I.N. with PBS. (A) Four weeks post-inoculation, the lungs were harvested from mice, and single-cell suspensions were prepared. PR8 virus NP-specific CD8$^+$ T cells in the lung tissues were identified using H-2D^b/ASNENMETM tetramer. (B) Four weeks post-inoculation, mice were challenged with 2 LD_{50} of HK68 virus. Three days post-challenge, the lungs were collected to determine viral titers. Data are a representation of two independent experiments. (C) Animals were euthanized at 3-day post-challenge, and the lung lobe samples were collected and processed for histopathology. The lung tissue sections in low magnification (H&E, 10×) are shown as insets on the left side of each higher magnification photo (H&E, 200×). At low magnification, darker foci correspond to areas with higher cellularity of inflammatory cells. At higher magnification, the lung sections with histopathology score from 0 (no histologic change) to 16 exhibit variably severe lesions, including suppurative bronchitis (asterisks), endarteritis/vasculitis (white arrowheads), hypertrophic vascular endothelium (black arrowhead), and peribronchiolar and perivascular inflammation (arrows). (D) Lung histopathology scores of the mice groups after challenge with A/Hong Kong/1/68(H3N2) (HK68) compared to the HAd-ΔE1E3-inoculated group. The mice inoculated with HAd-NPCD8 (10^7 PFU/animal) and HAd-NPCD8 (10^9 PFU/animal) show a statistically significant decrease in histopathology scores compared to the mice inoculated with HAd-ΔE1E3. (E) Three weeks post-inoculation with HAd-NP FL vectors, lung washes and sera were collected to determine recombinant PR8 NP-specific IgA and IgG titers by ELISA. ns, non-significant at $P > 0.05$; *, significant at $P < 0.05$; and **, significant at $P < 0.01$. Each experimental group consisted of at least five mice, and each experiment was repeated at least twice.

$\times 10^8$ and 1×10^9 PFU/mouse of the HAd-NPCD8 vector had similar numbers of NP-CD8$^+$ T cells, while mice infected with HAd-ΔE1E3 displayed only very low background staining (Fig. 4A). We also examined the histopathological changes in the lungs following the HK68 challenge and scored the changes in lungs from 0 (no histologic change) to 16, exhibiting variably severe lesions including suppurative bronchitis (asterisks), endarteritis/vasculitis (white arrowheads), hypertrophic vascular endothelium (black arrowhead), and peribronchiolar and perivascular inflammation (arrows) (Fig. 4C and D). The mice inoculated with HAd-NPCD8 (10^7 PFU/animal) and HAd-NPCD8 (10^9 PFU/animal) show a statistically significant decrease in histopathology scores compared to the mice inoculated with HAd-ΔE1E3.

Anti-NP mucosal IgA and serum IgG antibodies were detected by ELISA in mucosal washes and sera of mice inoculated with HAd-NP FL (Fig. 4E). However, no NP-specific antibodies were detected either in nasal secretions or sera of mice inoculated with HAd-NPCD8. Thus, increased frequency of NP-specific CD8$^+$ T cells results in enhanced viral clearance after heterosubtypic challenge in the absence of NP-specific antibodies.

Transcriptomic profiles of NP-specific CD8$^+$ T cells induced by different infection doses

The presence of a higher frequency of CD8$^+$ T cells aids in the recovery post-heterosubtypic virus challenge; however, it is not known if there are functional differences in terms of transcriptomic profiles between CD8$^+$ T cells induced by different doses of initial priming. To address this issue, we infected mice intranasally with 2 or 20 MID_{50} of the PR8 virus and boosted them with the same dose 2 weeks later. We harvested lung tissues 5 days post-boost, and NP-CD8$^+$ T cells were fluorescence activated cell sorter (FACS) sorted. We subjected an equal number of NP-specific CD8$^+$ T cells from mice immunized with high or low doses of PR8 virus for global RNA transcriptome analysis. There were 1,567 differentially expressed genes (DEGs) identified when we compared NP-CD8 $^+$ T cells between high and low doses of PR8 infection, which accounts for 6.63% of the total genes mapped (Fig. 5A). Among these, 888 genes were upregulated and 679 genes were downregulated. Gene Ontology (GO) functional and pathway enrichment analysis was performed using the clusterProfiler (19) package in R. NP-CD8$^+$ T cells induced by 20 MID_{50} PR8 virus, as compared to 2 MID_{50} infection dose, significantly enriched genes primarily associated with response to the virus, cytokine-mediated signaling, cell adhesion, and cell growth (Fig. 5B). Pathways associated with T cell function, including T cell proliferation and activation, regulation of immune effector process, actin filament organization, and migration were also substantially enriched in NP-CD8$^+$ T cells induced with the higher dose of infection. As shown in Fig. 5C, the expression of genes associated with the effector CD8$^+$ T cell response to virus infection, including CD8 T cell expansion and activation (CD86, CD63, CD81, Adam17, Pld2, Mertk, Mbp, and Irak1) and inflammatory cytokine production (IL-15), was upregulated in NP-CD8$^+$ T cells from mice infected with the higher dose of PR8.

Furthermore, increased expression of genes associated with CTL migration (Cxcl13, Ccl8, Cx3cr1, Alox5, and Rarα), clonal expansion, differentiation, survival (Rarα), and cytotoxicity effect (CD74, Vcam1, Cav1, Camp, and Prkcd) were observed in NP-CD8$^+$ T cells induced by the higher dose of PR8 infection. On the other hand, interferon-stimulated genes (Isg15 and Isg20), interferon regulatory factor 7 (Irf-7), interferon induced protein with tetratricopeptide repeats 3 (Ifit3b), known to be involved in type 1 IFN-mediated antiviral responses as shown in Fig. 4C, were significantly downregulated in response to the high dose of PR8 infection as compared to the low dose of PR8. Therefore, the comparative transcriptome analysis revealed a distinct gene profile of NP-CD8$^+$ T cells induced by the higher dose of HAd-NPCD8 associated with potent CTL function, which contributes to protective heterosubtypic immunity.

Metabolic pathways are essential regulators of immune differentiation, activation, and function and, as such, are central regulators of immune cell functions (20–22). Since changes in the metabolic profiles of immune cells are linked to altered functional

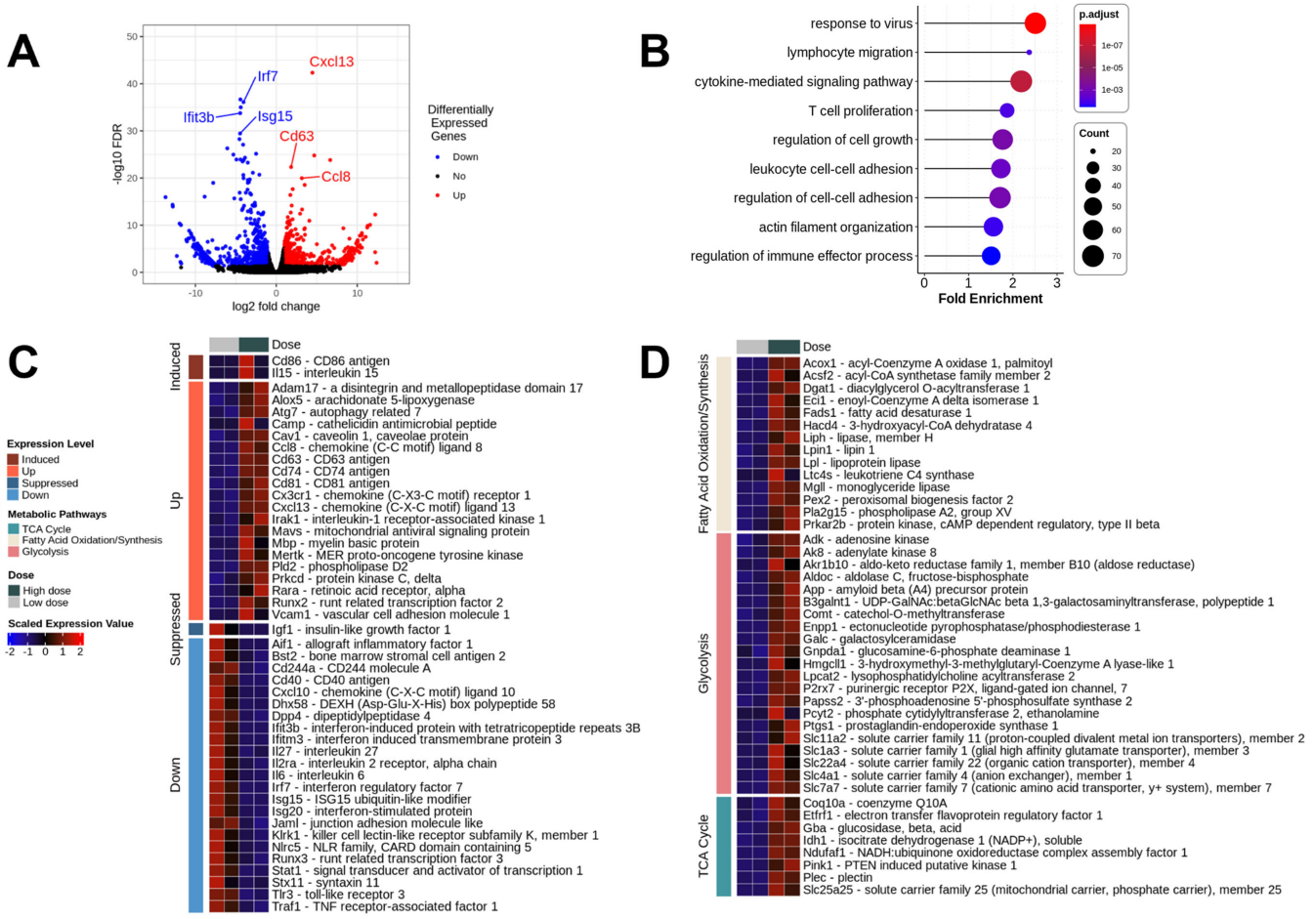

FIG 5 Transcriptomic profile of NP-CD8$^+$ T cells induced by different infection doses. NP-CD8$^+$ T cells from 10 to 15 mice each immunized with 2 or 20 MID_{50} PR8 viruses were sorted by FACS, and RNA content was sequenced with the Illumina platform. (A) Differentially expressed genes between the low- and high-dose groups are identified based on the adjusted *P*-value < 0.05 and |log2 fold change| > 1.0 from the DESeq2 analysis. The results are presented in a volcano plot. A total of 888 upregulated genes are shown in red and 679 downregulated genes are shown in blue. Essential genes among the top 10 based on adjusted *P*-value and fold change are labeled with gene symbols. (B) The 1,567 DEGs identified in the previous figure were analyzed for GO terms corresponding to the biological process. Among the 386 significantly enriched terms, top terms related to T cell functions were visualized in a bar plot. The length of the bars represents the count of genes associated with the GO term, and the color represents the adjusted *P*-value associated with the enrichment test. (C) The scaled expression values of key DEGs related to T cell functions between low- and high-dose groups are presented in a heatmap. Each column represents a sample in an experimental group, and each row represents a gene. Induced genes are genes with fold changes increased from zero under low-dose conditions to a positive value under high-dose conditions and vice versa for suppressed genes. (D) The scaled expression values of critical metabolic genes between the low- and high-dose groups are presented in a heatmap. Columns represent samples from low- and high-dose groups, and rows represent genes grouped by vital metabolic pathways, such as the glycolytic pathway, tricarboxylic acid (TCA) cycle, and fatty acid oxidation and synthesis. Both heatmaps were derived from RNA-seq experiments by comparing the RNA levels between the cells from a high and low dose with two biological replicates at each stage.

outcomes (23), we identified that 43 genes related to metabolic pathways are altered in the NP-CD8$^+$ T cells between high- and low-dose PR8 virus infection. NP-CD8$^+$ T cells from the high dose infection are characterized by the upregulation of genes involved in the glycolytic pathway, tricarboxylic acid cycle (TCA), and fatty acid metabolic pathways, indicating cells have altered cellular metabolic profile compared to cells obtained from the low dose of the virus. As shown in Fig. 5D, the commitment of the CD8$^+$ T cells from the high dose of virus infection toward glycolysis was reflected by the upregulation of genes involved in the glycolytic pathway, which included adenosine kinase (Adk) and aldolase C (AldoC), the key enzymes of the glycolytic pathway. Additionally, genes mapping to the TCA and mitochondrial electron transport chain,

electron transfer flavoprotein regulatory factor 1 (Etfrf1), NADH: ubiquinone oxidoreductase complex assembly factor 1 (Ndufaf1), coenzyme Q10A (Coq10a), as well as the fatty acid metabolism genes [Acyl-CoA synthetase family member 2 (Acsf2), Acyl-Coenzyme A oxidase 1, and palmitoyl (Acox1)], were also upregulated in the $CD8^+$ T cells isolated from the high virus dose. The gene expression changes support the observation that the cells from high and low virus doses are qualitatively different, with the cells from the high dose exhibiting higher expression of genes involved in the glycolytic pathway.

Functional characterization of NP-specific $CD8^+$ T cells induced by different infection doses

To further characterize the function of NP-specific $CD8^+$ T cells induced by different infectious doses, we stimulated an equal number of NP-specific $CD8^+$ T cells from lungs or spleens from mice infected with 2 or 20 MID_{50} of PR8 virus with NP peptide *in vitro* and examined their proliferation, cytokine production, and cytotoxic activity. NP-$CD8^+$ T cells induced by different infection doses displayed similar proliferation kinetics measured by carboxyfluorescein succinimidyl ester (CFSE) dilution (data not shown). However, NP-$CD8^+$ T cells from the spleen induced by a higher infection dose secreted significantly higher levels of IFN-γ and TNF-α as compared to those from mice infected with a lower dose of PR8 virus (Fig. 6A). A similar trend of cytokine production profile was detected in the NP-$CD8^+$ T cells isolated from the lungs, although the difference is not statistically significant (Fig. 6B). An equal number of NP-specific T cells from mice infected with 2 or 20 MID_{50} PR8 virus were co-cultured with CFSE-labeled EL4 cells pulsed with NP peptide to assess their cytotoxic activity. We determined the target cell death amount by quantifying 7-aminoactinomycin D (7-AAD)-positive EL4 cells. We observed two times higher 7-AAD^+ EL4 cells in co-cultures containing splenocytes from 20 MID_{50} infection dose compared to the co-culture containing splenocytes from 2 MID_{50} infection dose (22.2% ± 5.3% versus 52.24% ± 4.0%, Fig. 6C). Taken together, NP-$CD8^+$ T cells induced by higher PR8 infection dose displayed more cytokine production and cytotoxic activity. To further address the functional property of NP-$CD8^+$ T cells *in vivo*, an equal number of pooled NP-$CD8^+$ T cells isolated from lungs, lymph nodes, and spleens of mice infected with 2 or 20 MID_{50} PR8 viruses were adoptively transferred to naive mice. The antibodies used to characterize and gating strategy for lung and splenic NP-specific $CD8^+$ T cells are shown in Fig. S1 and S2, respectively. The transferred populations consist of similar frequencies of naive, central, and effector memory cell populations (Fig. S3). Mice were challenged with the HK68 virus 24 h later, and the viral titers in the lung were quantitated. The results presented in Fig. 6D demonstrated that mice receiving cells from 20 MID_{50} PR/8 dose had significantly lower viral load in the lung, as compared to mice receiving cells from 2 MID_{50} PR8, suggesting that NP-$CD8^+$ T cells induced by higher PR8 infection dose displayed more protective heterosubtypic immunity against the HK68 virus challenge. Therefore, besides the frequency, the functional quality of influenza NP-$CD8^+$ T cells is also critical for heterosubtypic immunity.

DISCUSSION

The seminal observation that adoptively transferred influenza-specific CTLs in mice can mediate influenza virus clearance by Yap et al. (24) in 1978 has led to an interest in delineating their role in mediating protection from influenza infection (25–29). Since CTLs recognize conserved epitopes (Fig. 2), developing vaccines that induce CTLs can confer protection against continuously evolving influenza viruses (30–34). In addition to viral clearance, influenza virus-specific $CD8^+$ T cells have been implicated in immunopathology in the lungs where the virus is replicating (35, 36). For example, when F5 TCR transgenic mice, which have a very high frequency of anti-influenza NP CTL precursors, were infected with different doses of influenza virus, exacerbated viral pathology and high mortality were observed only at high viral doses (37). In fatal cases with novel swine H1N1 influenza infection, Mauad et al. (38) showed the presence of many CTLs and granzyme B^+ cells within the human lung tissues. We examined whether $CD8^+$ CTL

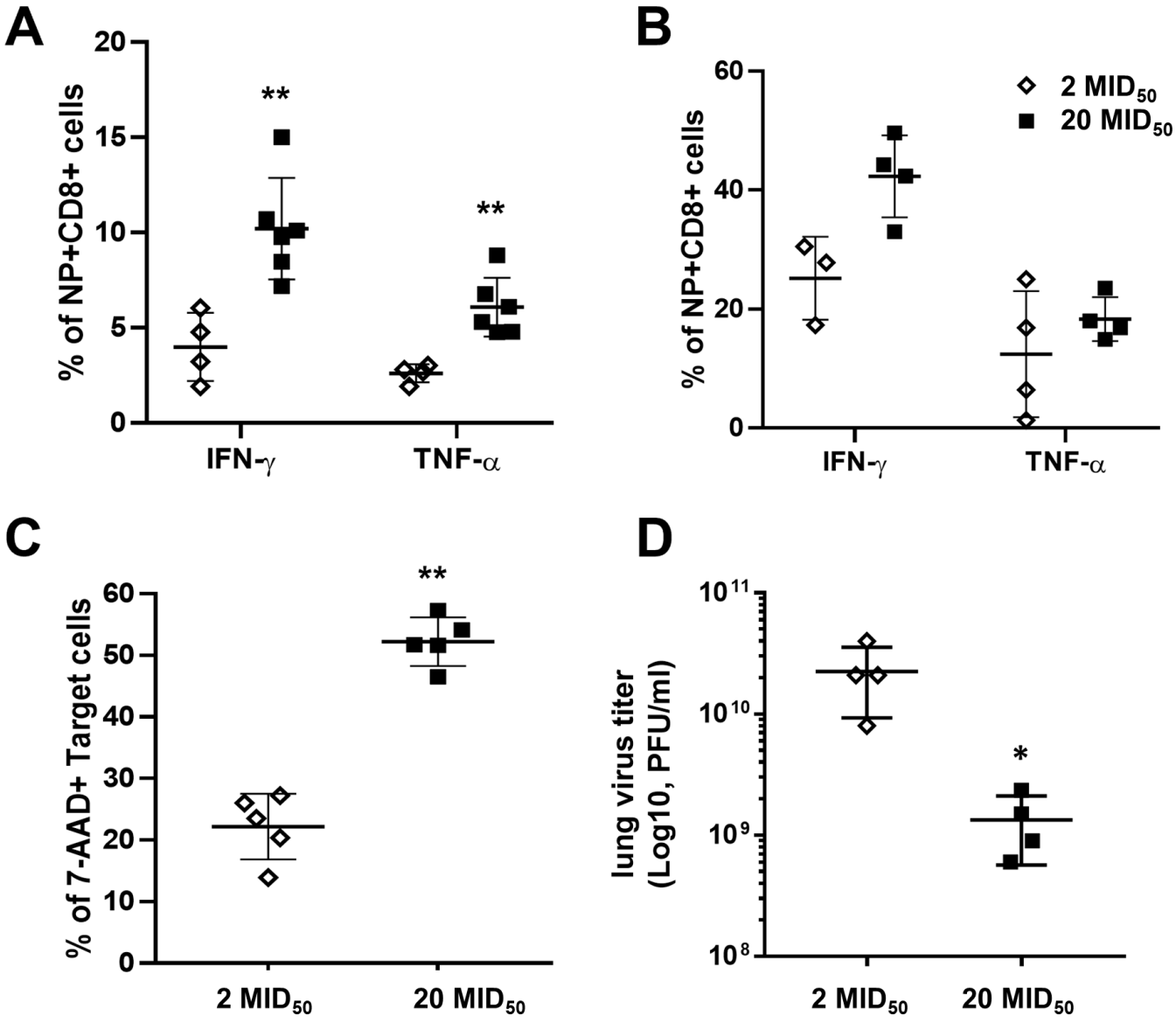

FIG 6 Functional characterization of NP-CD8$^+$ T cells induced by different infection doses. (A and B) Single-cell suspension of the lungs (A) and spleen (B) from 10 to 15 mice each infected with 2 or 20 MID_{50} PR8 virus for 3 weeks was *in vitro* stimulated with NP peptide (2 µM) in the presence of GolgiPlug for 12 h. The percentages of IFN-γ- or TNF-α-producing cells in the CD8$^+$ NP-tetramer$^+$ populations are presented. (C) Single-cell suspension of the spleens from mice infected with 2 or 20 MID_{50} PR8 virus for 3 weeks was *in vitro* stimulated with NP peptide for another 3 days and used as effector cells. EL4 cells pulsed with 2 µM of NP peptide and labeled with CFSE were used as target cells. Effector cells from the 2 MID_{50} dose were co-cultured with target cells at a ratio of 50:1. Adjusted amount of effector cells from the 20 MID_{50} dose was used for co-culture with target cells so that both groups have the same number of NP-CD8$^+$ T cells as effector cells. After 4 h of co-culture, 7-AAD was added to detect cell death. The percentages of 7-AAD$^+$ cells of total EL4 cells are presented. (D) NP-CD8$^+$ T cells were sorted from 10 to 15 mice each mouse infected with 2 or 20 MID_{50} PR8 virus for 2 weeks and boosted after 5 days. 5×10^5 cells were adoptively transferred to live mice via tail vein injection, and recipient mice were challenged with 2 LD_{50} HK68 virus 24 h later. Lung viral titer at day 5 post-challenge was determined by plaque assay. Data are a representation of two independent experiments. *$P < 0.05$ and **$P < 0.01$ compared to the 2 MID_{50} group.

frequency and/or function contribute to the protection and/or immunopathology following the heterosubtypic virus challenge.

We first used an infection-challenge model where mice were infected first with different doses (2, 10, or 20 MID_{50}) of an H1N1 (PR8) virus and then challenged with an H3N2 (HK68) virus. We observed that the frequency of reactive and cross-reactive NP-specific CD8$^+$ T cells is proportional to the virus infection dose before the challenge in the lymph node, spleen, and lung tissues. In addition, PR8-infected mice with increased

NP-CD8$^+$ T cells displayed enhanced survival and less morbidity against the H3N2 virus challenge compared to those that could only generate antibodies with low/no detectable levels of NP-CD8$^+$ T cells (I.M. immunization using FI PR8 virus) (Fig. 3A, B, and F). Furthermore, there was a dose-dependent clearance of the H3N2 virus in the lungs (Fig. 3G) with a corresponding decrease in pathological changes in the lungs (Fig. 3C). I.M. immunization with FI-PR8 and HK/68 challenge resulted in diffuse moderate to severe peribronchiolar and alveolar inflammation (score = 2–3). The severe tissue injury observed in the FI-PR8 group challenged with HK/68 is similar to those observed with the FI-RSV vaccine administered to children in 1960s, which resulted in severe inflammation of the lungs and case fatalities post-vaccination when exposed to RSV (39). It has been shown that formalin inactivation of RSV altered pre- and post-fusion protein ratios, which could lead to pathology (40). Subtle alterations and generation of reactive oxygen species tend to tilt the system toward Th2 responses and associated pathologies despite the protection (41). A similar observation was made with the FI Japanese B encephalitis vaccine and others (42). The enhanced pathology observed in the FI-PR8-immunized group compared to the PBS group may be due to the altered influenza viral antigens by formalin treatment. No structural or immunogenicity data exist comparing HA, NA, and M2e before and after formalin inactivation. Our findings suggest that an increased frequency of cross-reactive CD8$^+$ T cells does not cause immunopathology and appears to be critical for survival following heterosubtypic challenges. We employed a system that does not artificially increase the burst size of the NP-specific CD8$^+$ T cell response that happens in the adoptive transfer or transgenic models (37). Our findings also demonstrated a correlation between increased frequency of NP-specific CD8$^+$ T cells with enhanced survival upon heterosubtypic virus challenge. However, we could not rule out the contribution of non-HI but cross-reactive antibodies to other regions of HA, such as the stem, for survival upon heterosubtypic virus challenge (29, 43). To address this, we employed a replication-defective adenovirus expressing only the CD8$^+$ T cell epitope of the PR8 virus (HAd-NPCD8). Mice immunized with HAd-NPCD8 had no detectable anti-NP antibodies in the sera or nasal washes but generated NP-CD8$^+$ T cells, which protected mice against the HK68 virus challenge by reducing lung viral titers with corresponding reduction in lung pathology, which correlated with the frequency of NP-specific CD8$^+$ T cells (Fig. 4). Thus, antigen-specific CD8$^+$ T cells alone were sufficient and critical to recover from influenza without any antibody-mediated protective mechanisms. We further demonstrated that having a higher frequency of NP-specific CD8$^+$ T cells is crucial for heterosubtypic challenge.

The intrinsic quality of CTL has been shown to be as necessary as the frequency of CTL for the control and clearance of virus infection in adoptive transfer studies with HIV GP160-specific CD8$^+$ T cell lines induced with a recombinant vaccinia virus expressing GP160 and maintained *in vitro* by stimulating with peptides. Adoptive transfer of established CD8$^+$ T cell lines that have either high or low avidity as determined by anti-CD3 antibody-redirected lysis of Fc-receptor-expressing target cells, P815, demonstrated that low avidity CD8$^+$ T cells were inefficient in clearing recombinant vaccinia virus infection (14). These findings prompted us to examine whether influenza NP-CD8$^+$ T cells induced by a high virus dose are qualitatively different from the ones induced by a lower virus dose. Our study used CD8$^+$ T cells induced *in vivo* without subsequent *in vitro* manipulation or culture. Next, we observed significant differences in transcriptomics signatures between NP-specific T cells induced by different doses of PR8 infection. Specifically, 888 genes were significantly upregulated by higher doses of PR8, while 679 genes were substantially downregulated.

Upon influenza infection, naive CD8$^+$ T cells are primed by antigen-presenting cells in secondary lymphoid organs, which leads to CD8$^+$ T cell activation and expansion. Activation of CD8$^+$ T cells depends on three signals: TCR engagement (signal 1), costimulatory (signal 2), and inflammatory stimulus (signal 3) (44). The functional annotation analysis of NP-CD8$^+$ T cells for enrichment of GO Biological Process (BP) terms identified 386 significantly enriched terms with adjusted *P*-value < 0.05. Among

these, 159 (41.2%) enriched GO terms are related to T cell functions. These results demonstrated that a high dose of PR8 increased the expression of pathways necessary for $CD8^+$ T cell activation and expansion, including pathways response to the virus, cytokine-mediated signaling, regulation of cell growth, and cell-cell adhesion (Fig. 5B). Specifically, the induction of CD86 and upregulation of CD63, CD81, Mbp, and Mertk was observed on NP-$CD8^+$ T cells from mice infected with the higher dose of PR8 virus. These molecules were shown to be critical for $CD8^+$ effector function as costimulatory or activation molecules (45–49). The inflammatory cytokine IL-15 was reported to induce $CD8^+$ T cells to acquire functional NK receptors capable of modulating cytotoxicity and cytokine secretion. A higher dose of PR8 significantly induced this gene compared to a lower dose (50). After activation, T cells undergo clonal expansion and gain different effector functions. The expression of genes Adam17, Pld2, and Irak1 was substantially increased in NP-$CD8^+$ T cells from the high-dose group. Several studies have reported that these genes are involved in $CD8^+$ T cell proliferation (51–53). Upon activation, $CD8^+$ T cells exit the lymph node and home toward inflamed tissues under the guidance of adhesion and chemokine expressed by the inflamed tissue (54). Cxcl13 and Ccl8 mediate the recruitment of $CD8^+$ T cells to control viral infection (55–57). Similarly, Rarα plays an important role in the homing of T cells, their differentiation, expansion, and survival as Rarα-deficient $CD8^+$ T cells failed to control *Listeria monocytogenes* infection (58, 59). *In vitro* studies demonstrated the critical role of Cx3cr1 in effector lymphocyte trafficking (60). In our study, the increased expression of these genes in NP-$CD8^+$ T cells from the high dose of PR8 indicates the efficient trafficking of activated $CD8^+$ T cells toward the infection site to combat the pathogen (55, 56, 58–60). The CTLs target virus-infected host cells and kill them through three known mechanisms: perforin/granzyme-mediated cytolysis, apoptosis mediated by FasL/Fas, and TRAIL/TRAIL-DR signaling (54). Related genes associated with the cytotoxicity killing, such as CD74, Vcam1, Cav1, Camp, and Prkcd, were upregulated by the higher infection dose. While CD74, Camp, and VCAM-1 were demonstrated to boost $CD8^+$ T cell immunity (61, 62), Cav1 was reported to modulate CD8+ effector function through membrane organization and integrin function (63), and Prkcd directly mediates TCR signals leading to granule exocytosis-mediated cytotoxicity (64). It has been shown that innate immune response genes in adaptive immune cells, such as $CD8^+$ T cells, are modulated in acute and chronic infections to induce antiviral or anti-tumor responses (57, 65, 66). Isg15, Isg20, Irf7, and Ifit3b play a significant role in antiviral immunity mediated by type 1 IFN induced by innate immune sensors (67). However, they are downregulated in activated $CD8^+$ T cells induced by high-dose PR8 virus. These $CD8^+$ T cells are likely programmed to perform a lytic function, as demonstrated in Fig. 5C, compared to the $CD8^+$ T cells induced by the low-dose virus, which may rely on conventional lytic function and innate immune responses. Investigation of kinetics of induction and activation of CD8+ T cells in response to antigen dose at transcriptome and proteome levels will delineate the role of innate genes in $CD8^+$ T cell-mediated heterosubtypic immunity. Changes in the antigen-presenting cells, priming microenvironment, and cytokine milieu may contribute to the observed changes in $CD8^+$ T cells. For example, Boon et al. (68) demonstrated that the concentration of IL-2 during *in vitro* expansion of influenza M1- and NP-specific cells had a profound effect on their functionality.

Metabolic reprogramming of innate immune cells influences the functions and differentiation of immune cells and the course of an immune response (20–22, 69–72). Recent evidence suggests that different classes of T cells have distinct metabolic profiles to meet the cells' energy demands. For example, naive T cells use glucose and fatty acid as an energy source, activated T cells are known to upregulate glycolytic pathways even in the presence of sufficient oxygen, effector T cells are more dependent on glucose, and memory T cells use fatty acid oxidation. Here, we have shown that $CD8^+$ T cells from the high antigen dose have an altered bioenergetic profile compared to $CD8^+$ T cells induced by a low-dose antigen. To gain insight into the molecular basis for observed different effects of the two different antigen doses on the functional outcome of the

CD8$^+$ T cells, we examined the role of glycolysis during the induction/activation of CD8$^+$ T cells. Our results show that glycolytic enzymes are upregulated in CD8$^+$ T cells. These findings reveal that modifications of metabolic glycolytic and OXPHos pathways regulate the cellular functions of CD8$^+$ T cells. To further characterize the functional properties of NP-CD8$^+$ T cells, memory CD8+ T cells were generated upon infection with 2 or 20 MID_{50} of the PR8 virus. Cells were then re-stimulated *in vitro* using NP peptide to recall NP-specific CD8$^+$ T cell response. The recall proliferation potential of NP-CD8$^+$ T cells was monitored by CFSE dilution, and no difference was observed between NP CD8$^+$ T cells induced by two infection doses. However, spleen and lung NP-CD8$^+$ T cells from mice infected with 20 MID_{50} PR8 produced substantially higher levels of IFN-γ- and TNF-α-secreting cells, compared to NP-CD8$^+$ T cells induced by a lower infection dose. High infection dose programmed CD8$^+$ T cells differently than the low infection dose, with genes involved in glycolytic pathways being highly expressed in cells induced by the high dose signifying their functional differences.

Furthermore, NP-CD8$^+$ T cells from higher infection doses demonstrated significantly more cytotoxic activity. The *in vivo* transfer study directly demonstrated that NP-CD8$^+$ T cells from mice infected with 20 MID_{50} PR8 provide better protective immunity than the same number of NP-CD8$^+$ T cells from mice infected with 2 MID_{50} PR8 when an equal number of them were transferred, and the naive, central, and effector memory composition of the adoptively transferred cells is similar. NP is highly conserved among influenza A virus strains, and NP-specific CTLs can confer protective immunity against antigenically distinct influenza A virus strains (73, 74). Therefore, in our model, NP-specific CD8$^+$ CTLs induced by PR8 infection or HAd-NP vaccination cleared HK68-infected cells and conferred heterosubtypic protection.

In conclusion, influenza-virus-specific CD8$^+$ T cells are critical for survival from heterosubtypic challenges without causing immunopathology. Furthermore, the functional quality and frequency of CD8$^+$ T cells are both crucial in conferring heterosubtypic protection. Hence, developing next-generation influenza vaccines that can induce/recall humoral immune responses and enhanced frequency with the quality of CD8$^+$ T cells is crucial to control epidemics and pandemics.

MATERIALS AND METHODS

Generation and characterization of replication-defective HAd-NPCD8, HAd-NP FL, and HAd-ΔE1E3 vectors

HAd-NPCD8, HAd-NP FL, and HAd-ΔE1E3 vectors were constructed as described previously (75) Briefly, HAd-NP FL or HAd-NPCD8 represents HAd-ΔE1E3 expressing either the full-length coding region of the NP gene of the PR8 influenza virus or one of the NP CD8 epitopes of the PR8 virus (366–374, ASNENMETM), respectively. The gene construct was under the control of cytomegalovirus promoter and bovine growth hormone polyadenylation signal (polyA). HAd-ΔE1E3 represents the E1 and E3 deleted HAd vector. The vectors were plaque purified, and their genomes were analyzed by restriction enzyme digestion and sequencing to confirm the presence or absence of a foreign gene cassette. HAd-ΔE1E3, HAd-NP FL, or HAd-NPCD8 were grown in HEK 293 cells (76), purified by cesium chloride density-gradient centrifugation (76), and titrated by PFU assay in BHH-2C (bovine human hybrid 2C) cells (77).

Influenza viruses

Influenza viruses used in this study include A/Puerto Rico/8/34 (PR8, H1N1) and A/Hong Kong/1/68 (HK68, H3N2). Viruses were propagated for 2 days in the allantoic cavity of 10-day-old embryonated chicken eggs. Pooled allantoic fluid was clarified by centrifugation, sequenced, titered, aliquoted, and stored at −80°C until use.

Immunization and virus infections

Six-week-old female C57BL/6 mice (Jackson Laboratory, Bar Harbor, ME, USA) were anesthetized by inhalation of isoflurane and infected intranasally with 2, 10, and 20 MID_{50} of PR8 virus in a final volume of 50 µL. Similarly, mice were immunized I.N. with various doses of (1×10^6, 1×10^7, 1×10^8, and 1×10^9 PFU/mouse) replication-deficient adenoviruses, HAd-NPCD8, HAd-NP FL, or HAd-ΔE1E3. In addition, control mice were immunized intramuscularly with 500 hemagglutinin units in 50 µL of formalin-inactivated PR8 virus in each quadriceps muscle. Sera were obtained 3 weeks post-infection/immunization to determine antibody responses. Four weeks post-infection/immunization, mice were challenged with 2 50% lethal dose (2 LD_{50}) of HK68 (H3N2) influenza virus and monitored for weight loss and mortality or lung virus titers. For RNA sequencing analysis, mice were infected I.N. with 2 or 20 MID_{50} of the PR8 virus and boosted with the same dose 2 weeks later. Lung tissues were harvested 5 days post-boost, and NP-$CD8^+$ T cells were FACS sorted. Mice losing more than 25% of their pre-infection body weight were humanely euthanized.

Flow cytometry and cell sorting

Mice received a 100 µL intravenous (IV) injection retro-orbitally of 1 µg fluorescently conjugated CD45 (IV-label) 5 min prior to sacrifice to delineate cells in circulation versus those that are tissue-resident. Lung tissues were harvested at sacrifice into gentleMACS c-tubes (Miltenyi) containing 2.4 mL of serum-free 1× RPMI-1640 (Gibco) supplemented with 2 mM L-glutamine, 1 mM sodium pyruvate, 1× nonessential amino acids, 1× antibiotic/antimycotic solution (all from Corning; sf-RPMI-1640), along with a final concentration of 10 mg/mL Liberase TL (Roche) and 100 mg/mL DNase1 (Sigma) at 4°C. Tissues were homogenized using a gentleMACS Octo Dissociator with two cycles of the m_lung_01_02 protocol, each followed by a 10-min incubation at 37°C. Following the second 10-min incubation, c-tubes were returned to the dissociator and the m_lung_02_01 protocol was run followed by a 10-min incubation at 37°C. After the last 10-min incubation at 37°C (30 min in total), the c-tubes were returned to the dissociator and the m_lung_01_02 protocol and m_lung_02_01 protocol were run in immediate succession. Cells were then pelleted by centrifugation for 5 min at 1,400 rpm and 4°C and then the lung digestion supernatant was aspirated off. Cells were resuspended in 10 mL of a custom deficient RPMI-1640 media containing 3% newborn calf serum (NBCS; Life Technologies) and 0.1 µL/mL Benzonase (Sigma; hereafter FACS buffer) and passed through a 70 µm cell strainer (Miltenyi). Single-cell suspensions were pelleted and resuspended in 1 mL of ammonium-chloride-potassium (ACK) lysis buffer to lyse red blood cells (RBCs) for ~2 min at room temperature (RT). Following RBC lysis, 10 mL FACS buffer was added, and cells were pelleted through a 2 mL 100% NBCS serum layer prior to downstream processing.

Spleen cells were passed through a 70 µm cell strainer to obtain single-cell suspensions, and RBCs were lysed with ACK lysis buffer. Following RBC lysis, 10 mL FACS buffer was added, and cells were pelleted through a 2 mL 100% NBCS serum layer prior to downstream processing.

Cells (up to 10^7 total) were resuspended in 44 µL FACS buffer and pre-incubated with 1 µL TruStain FcX (BioLegend) and 5 µL CellBlox (ThermoFisher Scientific; final volume 50 µL) for 10 min at 4°C in 5 mL FACS tubes (Corning). The 20-color extracellular staining master mix (Fig. S1) was prepared 2× in BD Horizon Brilliant Stain Buffer (BD Biosciences), added 1:1 (50 µL) to cells, and then incubated for 30 min at 4°C. Following staining, cells were washed with ~4 mL of FACS buffer. Cells were fixed in 1.6× BD FACS lysing solution (10× stock diluted in dH_2O) for 30 min at room temperature. Cells were washed in ~4 mL FACS buffer, then resuspended in 200–1,000 µL FACS buffer with 10 µL of Precision Count Beads (BioLegend) for acquisition using BD FACSDiva Software on a BD FACSymphony A5. To distinguish auto-fluorescent cells from cells expressing low levels of a particular surface marker, we established upper thresholds for auto-fluorescence

by staining samples with fluorescence-minus-one control stain sets in which a reagent for a channel of interest is omitted. Data were analyzed with FlowJo version 10.8.1 (BD Biosciences). Mice received a 100 µL IV injection retro-orbitally of 1 µg fluorescently conjugated CD45 (IV-label, see Fig. S2) 5 min prior to sacrifice to delineate cells in circulation versus those that are tissue-resident. Lung tissues were harvested at sacrifice into gentleMACS c-tubes (Miltenyi) containing 2.4 mL of serum-free 1× RPMI-1640 (Gibco) supplemented with 2 mM L-glutamine, 1 mM sodium pyruvate, 1× nonessential amino acids, 1× antibiotic/antimycotic solution (all from Corning; sf-RPMI-1640), along with a final concentration of 10 mg/mL Liberase TL (Roche) and 100 µg/mL DNase1 (Sigma) at 4°C. Tissues were homogenized using a gentleMACS Octo Dissociator with two cycles of the m_lung_01_02 protocol, each followed by a 10-min incubation at 37°C. Following the second 10-min incubation, c-tubes were returned to the dissociator and the m_lung_02_01 protocol was run followed by a 10-min incubation at 37°C. After the last 10-min incubation at 37°C (30 min in total), the c-tubes were returned to the dissociator and the m_lung_01_02 protocol and m_lung_02_01 protocol were run in immediate succession. Cells were then pelleted by centrifugation for 5 min at 1,400 rpm and 4°C and then the lung digestion supernatant was aspirated off. Cells were resuspended in 10 mL of a custom deficient RPMI-1640 media [see reference (4)] containing 3% newborn calf serum (Life Technologies) and 0.1 µL/mL Benzonase (Sigma; hereafter FACS buffer) and passed through a 70 µm cell strainer (Miltenyi). Single-cell suspensions were pelleted and resuspended in 1 mL of ACK lysis buffer to lyse red RBCs for ~2 min at room temperature. Following RBC lysis, 10 mL FACS buffer was added, and cells were pelleted through a 2 mL 100% NBCS serum layer prior to downstream processing.

Spleen cells were passed through a 70 µm cell strainer to obtain single-cell suspensions, and RBCs were lysed with ACK lysis buffer. Following RBC lysis, 10 mL FACS buffer was added, and cells were pelleted through a 2 mL 100% NBCS serum layer prior to downstream processing. PR8 or HK68-specific NP $CD8^+$ T cells in the lungs, lymph nodes, and spleens were identified using H-$2D^b$/ASNENMETM or H-$2D^b$/ ASNENMDAM tetramer, respectively (NIH tetramer core facility, Emory University, Atlanta, GA, USA). 1×10^6 cells from the lung and spleen of mice infected with the PR8 virus for 3 weeks were stimulated *in vitro* with NP peptide (2 µM) for 12 h with GolgiPlug (BD Bioscience, San Jose, CA, USA) to detect intracellular cytokine production. Cells were surface stained with anti-CD44, anti-CD8 antibody, and NP tetramer, followed by intracellular staining with anti-IFN-γ and anti-TNF-α antibody (BD Bioscience). Splenocytes from mice infected with the PR8 virus for 3 weeks were labeled with 5 µM carboxyfluorescein succinimidyl ester and incubated with NP peptide for 5 days. Cells were then surface stained with CD8 and NP tetramer. Samples were analyzed using an LSR Fortessa Flow cytometer (BD Biosciences), and the cytometric data were analyzed using FlowJo software version 9.3.3 (Tree Star, Inc). For adoptive transfer experiments, two groups each of 15–20 mice were infected with either 2 or 20 MID_{50} PR8 virus and boosted 2 weeks later. Lung, lymph node, and spleen were harvested 5 days post-boost pooled from 15 to 20 mice for each virus dose, and NP $CD8^+$ T cells were sorted using a FACS Aria II (BD). 5×10^5 sorted cells were then adoptively transferred via the tail vein in 100 µL volume to each recipient mouse.

In vitro cytotoxicity assay

Effector cells were prepared from the spleens of mice infected with 2 or 20 MID_{50} PR8 virus for 7 days or spleens of mice infected for 21 days and expanded *in vitro* with NP peptide (2 µM) for another 3 days. Target cells EL4 were pulsed with NP peptide for 1 h each at 26°C and 37°C and then labeled with 5 µM of CFSE. Effector and target cells were co-cultured at a 50:1 (E/T) ratio for 4 h and then stained with 7-aminoactinomycin D (BD Biosciences) for 30 min. Cells were acquired on an LSR Fortessa Flow cytometer to detect the death of EL4 cells as an indication of $CD8^+$ T cell-mediated killing.

Quantitation of viral titers in the lung

Lung tissues were harvested 5 days post-challenge and homogenized in 2 mL of cold PBS. Confluent monolayers of MDCK cells in 6-well plates were washed with DMEM and infected with serial 10-fold dilutions of lung homogenates for 1 h at 37°C in 5% CO_2. Cells were washed with DMEM and overlayed with 1.6% SeaKem LE agarose (Lonza, Basel, Switzerland) mixed 1:1 with 2× L15 medium (Lonza, Basel, Switzerland) containing 4 mM 4-(2-hydroxyethyl)-1-piperazineethanesulfonic acid, 2 mM L-glutamine, 5 µg/mL gentamycin, 1.5 mg/mL sodium bicarbonate, and 1 µg/mL TPCK-treated trypsin (Sigma-Aldrich, St. Louis, MO, USA). Virus plaques were stained with 0.3% crystal violet solution (BD, Sparks, MD, USA) after 72-h incubation at 37°C in 5% CO_2 and counted.

Antibody assays

Sera collected from immunized mice were treated with receptor-destroying enzyme (RDE, Denka Seiken) at 37°C overnight and titered against PR8 and HK68 viruses by the standard HI assay using 1% turkey RBCs. Briefly, 25 µL of 1× PBS was added to wells of a 96-well V-bottom plate (Corning). This was followed by adding 50 µL of RDE-treated sera to each column and then serially diluted. Next, 25 µL of 4 HA units of PR8 or HK68 virus was added to each well and incubated at RT for 30 min. Finally, 50 µL of 1% standardized turkey RBCs in PBS was added to each well and incubated at RT for exactly 30 min. The reciprocal serial dilutions of the sera that showed complete inhibition of hemagglutination were recorded as the HI titer. NP antigen-specific ELISA was performed to determine IgA and IgG antibody titers in sera and lung washes.

Histopathology

On the designated days post-viral challenge, the lung samples were collected and fixed in 10% neutral buffered formalin. After 72 h, the samples were transferred to 70% ethanol, sectioned, and stained with H&E. The lung pathology scores are with the following description: 0, no inflammation; 1, mild inflammation; 2, moderate inflammation; and 3, severe inflammation.

RNA isolation, sequencing, alignment, and quantification

RNA samples were purified from 10^5 FACS-sorted NP-$CD8^+$ T cells with Direct-zol Microprep kit (Zymo, CA, USA). RNA concentration was measured by Bioanalyzer 2100 with Agilent RNA 6000 Pico kit (Agilent, CA, USA). Thirteen nanograms of total RNA (RIN 6.8–7.9) was used for the construction of NGS libraries with QIAseq FX Single Cell RNA Library Kit (Qiagen, MD, USA). The libraries were quantified by Bioanalyzer 2100 with Agilent High Sensitivity DNA Kit (Agilent, CA, USA) and sequenced on a NovaSeq6000 system with NovaSeq 6000 SP reagent kit v1 (100 cycles) (Illumina, CA, USA). Sequences were mapped to the mm10 Mus musculus Ensembl Transcriptome v96 and quantified using Kallisto (78) and Taximport (79).

Differential expression analysis

Differential expression analysis was performed in R with the package DESeq2 (80–82). Transcripts that have more than five mapped reads in at least two samples were kept for analysis. Genes with low counts were filtered for low expression by their normalized mean counts, and raw *P*-values were adjusted for multiple testing using the Benjamini-Hochberg correction. Genes considered significantly differentially expressed are those that passed the filters: (i) adjusted *P*-values controlled at false discovery rates (FDR) < 0.05 threshold; and (ii) the absolute value of $\log_2$ fold change > 1. A volcano plot was produced in the R with the package ggplot2 (83) and showed the $\log_2$ fold change of each gene plotted against its false discovery rate (–log10FDR), both of which were calculated in DESeq2. Enrichment of all DEGs in BP GO terms was analyzed in R with the package clusterProfiler (19), and the top enriched GO terms are visualized in a bar

plot. A subset of 46 important DEGs was selected to generate the heatmap in R with the package ComplexHeatmap (84). Processed data and code are available via link: yyw-informatics/RNA-seq-InfluenzaNP-CD8-T-cells (github.com).

Statistical analysis

Statistical analysis was performed using GraphPad Prism software (GraphPad Software). A one-way ANOVA with multiple comparisons was used to determine the significance of the NP-specific $CD8^+$ T cell data and HI titer among all groups. In addition, the Student's *t*-test was used to analyze differences among treatments for intracellular cytokine production, *in vitro* cytotoxicity assay, and virus titer. Data were presented as mean ± SEM. All differences were considered significant when the *P*-value was ≤0.05.

ACKNOWLEDGMENTS

We thank the NIH Tetramer Core Facility at Emory University for providing reagents for this study.

Studies carried out at Purdue University were supported by Public Health Service grant AI059374 from the National Institute of Allergy and Infectious Diseases and the Hatch Fund to S.K.M., and investigations at the Centers for Disease Control and Prevention were carried out by intramural funding.

The findings and conclusions in this report are those of the authors and do not necessarily represent the views of the Centers for Disease Control and Prevention.

S.S., S.A., W.C., E.E.S., and W.-C.W. designed and performed experiments. E.E.S., W.-C.W. and S.K.M. constructed, characterized, purified, and titrated HAd-ΔE1E3, HAd-NP FL, and HAd-NPCD8. W.S. and N.W. performed lung section histopathology. S.R. and D.J.E. performed flow cytometry and in vitro cytotoxicity assays. A.K. quantitated the viral titers in the lungs and A.K. and S.D.S. performed HI assays. C.B. performed the mice adoptive transfer studies. P.R. purified RNA for sequencing. M.M., M.S., J.H., R.A., J.L., J.P., M.B., and R.J. performed RNA sequencing. Y.W., R.A., and R.J. performed data analysis. S.G. assisted and ensured that the animal experiments are carried out as per the protocols.

AUTHOR AFFILIATIONS

[1]Influenza Division, National Center for Immunization and Respiratory Diseases, Centers for Disease Control and Prevention, Atlanta, Georgia, USA
[2]Department of Comparative Pathobiology, Purdue University, West Lafayette, Indiana, USA
[3]Biotechnology Core Facility Branch, Division of Scientific Resources, National Center for Emerging and Zoonotic Infectious Diseases, Centers for Disease Control and Prevention, Atlanta, Georgia, USA
[4]Division of High Consequence Pathogens and Pathology, National Center for Emerging and Zoonotic Infectious Diseases, Centers for Disease Control and Prevention, Atlanta, Georgia, USA
[5]Department of Biology, Georgia State University, Atlanta, Georgia, USA
[6]Emory Integrated Computational Core, Emory Integrated Core Facilities, Emory University, Atlanta, Georgia, USA
[7]Indiana Animal Disease Diagnostic Laboratory, Department of Comparative Pathobiology, Purdue University, West Lafayette, Indiana, USA
[8]Department of Human Genetics, Emory University School of Medicine, Emory University, Atlanta, Georgia, USA

AUTHOR ORCIDs

Suresh K. Mittal http://orcid.org/0000-0001-8475-8449
Suryaprakash Sambhara http://orcid.org/0000-0002-4715-5793

FUNDING

Funder	Grant(s)	Author(s)
National Institutes of Health	AI059374	Suresh K. Mittal

AUTHOR CONTRIBUTIONS

Samuel Amoah, Formal analysis, Investigation, Writing – original draft | Weiping Cao, Conceptualization, Formal analysis, Investigation, Methodology, Writing – review and editing | Ekramy E. Sayedahmed, Formal analysis, Investigation, Methodology | Yuanyuan Wang, Formal analysis, Visualization, Writing – review and editing | Amrita Kumar, Formal analysis, Investigation | Margarita Mishina, Formal analysis, Investigation, Methodology | Devon J. Eddins, Formal analysis, Investigation, Methodology, Visualization | Wen-Chien Wang, Formal analysis, Investigation | Mark Burroughs, Formal analysis | Mili Sheth, Formal analysis, Methodology | Justin Lee, Formal analysis, Methodology | Wun-Ju Shieh, Formal analysis, Investigation | Sean D. Ray, Formal analysis, Investigation | Caitlin D. Bohannon, Investigation, Methodology | Priya Ranjan, Formal analysis, Investigation | Jessica Hoehner, Formal analysis | Robert A. Arthur, Formal analysis | Shivaprakash Gangappa, Formal analysis, Investigation, Methodology, Supervision | Nobuko Wakamatsu, Formal analysis | H. Richard Johnston, Formal analysis | Jan Pohl, Formal analysis, Methodology, Supervision | Suresh K. Mittal, Formal analysis, Methodology, Supervision | Suryaprakash Sambhara, Conceptualization, Funding acquisition, Methodology, Project administration, Resources, Writing – original draft, Writing – review and editing.

DATA AVAILABILITY

The data that support the findings of this study are available on request from the corresponding author, S.S.

ETHICS APPROVAL

Animal research was conducted using the guidelines of the CDC's Institutional Animal Care and Use Committee in the Association for Assessment and Accreditation of Laboratory Animal Care International (AAALAC), an accredited animal facility.

ADDITIONAL FILES

The following material is available online.

Supplemental Material

Figure S1 (JVI00711-24-s0001.tif). List of antibodies used.
Figure S2 (JVI00711-24-s0002.tif). Gating strategy.
Figure S3 (JVI00711-24-s0003.tif). Naïve, central memory (CM), and effector memory (EM) cells.

REFERENCES

1. Iuliano AD, Roguski KM, Chang HH, Muscatello DJ, Palekar R, Tempia S, Cohen C, Gran JM, Schanzer D, Cowling BJ, et al. 2018. Estimates of global seasonal influenza-associated respiratory mortality: a modelling study. Lancet 391:1285–1300. https://doi.org/10.1016/S0140-6736(17)33293-2
2. WHO. 2018. Seasonal influenza fact sheet. Available from: http://www.who.int/news-room/fact-sheets/detail/influenza-(seasonal). Retrieved 24 May 2018.
3. Palladino G, Mozdzanowska K, Washko G, Gerhard W. 1995. Virus-neutralizing antibodies of immunoglobulin G (IgG) but not of IgM or IgA isotypes can cure influenza virus pneumonia in SCID mice. J Virol 69:2075–2081. https://doi.org/10.1128/JVI.69.4.2075-2081.1995
4. Steinhauer DA, Domingo E, Holland JJ. 1992. Lack of evidence for proofreading mechanisms associated with an RNA virus polymerase. Gene 122:281–288. https://doi.org/10.1016/0378-1119(92)90216-c
5. Rajão DS, Pérez DR. 2018. Universal vaccines and vaccine platforms to protect against influenza viruses in humans and agriculture. Front Microbiol 9:123. https://doi.org/10.3389/fmicb.2018.00123
6. Kreijtz JHCM, Bodewes R, van den Brand JMA, de Mutsert G, Baas C, van Amerongen G, Fouchier RAM, Osterhaus ADME, Rimmelzwaan GF. 2009. Infection of mice with a human influenza A/H3N2 virus induces protective immunity against lethal infection with influenza A/H5N1 virus. Vaccine 27:4983–4989. https://doi.org/10.1016/j.vaccine.2009.05.079
7. Kreijtz JHCM, Bodewes R, van Amerongen G, Kuiken T, Fouchier RAM, Osterhaus ADME, Rimmelzwaan GF. 2007. Primary influenza A virus

infection induces cross-protective immunity against a lethal infection with a heterosubtypic virus strain in mice. Vaccine 25:612–620. https://doi.org/10.1016/j.vaccine.2006.08.036
8. Nguyen HH, Moldoveanu Z, Novak MJ, van Ginkel FW, Ban E, Kiyono H, McGhee JR, Mestecky J. 1999. Heterosubtypic immunity to lethal influenza A virus infection is associated with virus-specific CD8(+) cytotoxic T lymphocyte responses induced in mucosa-associated tissues. Virology 254:50–60. https://doi.org/10.1006/viro.1998.9521
9. McMichael AJ, Gotch FM, Noble GR, Beare PA. 1983. Cytotoxic T-cell immunity to influenza. N Engl J Med 309:13–17. https://doi.org/10.1056/NEJM198307073090103
10. Yewdell JW, Bennink JR, Smith GL, Moss B. 1985. Influenza A virus nucleoprotein is a major target antigen for cross-reactive anti-influenza A virus cytotoxic T lymphocytes. Proc Natl Acad Sci U S A 82:1785–1789. https://doi.org/10.1073/pnas.82.6.1785
11. Gotch F, McMichael A, Smith G, Moss B. 1987. Identification of viral molecules recognized by influenza-specific human cytotoxic T lymphocytes. J Exp Med 165:408–416. https://doi.org/10.1084/jem.165.2.408
12. Kees U, Krammer PH. 1984. Most influenza A virus-specific memory cytotoxic T lymphocytes react with antigenic epitopes associated with internal virus determinants. J Exp Med 159:365–377. https://doi.org/10.1084/jem.159.2.365
13. Sridhar S, Begom S, Bermingham A, Hoschler K, Adamson W, Carman W, Bean T, Barclay W, Deeks JJ, Lalvani A. 2013. Cellular immune correlates of protection against symptomatic pandemic influenza. Nat Med 19:1305–1312. https://doi.org/10.1038/nm.3350
14. Alexander-Miller MA, Leggatt GR, Berzofsky JA. 1996. Selective expansion of high- or low-avidity cytotoxic T lymphocytes and efficacy for adoptive immunotherapy. Proc Natl Acad Sci U S A 93:4102–4107. https://doi.org/10.1073/pnas.93.9.4102
15. Calin-Laurens V, Trescol-Biémont MC, Gerlier D, Rabourdin-Combe C. 1993. Can one predict antigenic peptides for MHC class I-restricted cytotoxic T lymphocytes useful for vaccination? Vaccine 11:974–978. https://doi.org/10.1016/0264-410x(93)90389-f
16. Jong P, Gong Y, Liu PP, Austin PC, Lee DS, Tu JV. 2003. Care and outcomes of patients newly hospitalized for heart failure in the community treated by cardiologists compared with other specialists. Circulation 108:184–191. https://doi.org/10.1161/01.CIR.0000080290.39027.48
17. Valkenburg SA, Gras S, Guillonneau C, La Gruta NL, Thomas PG, Purcell AW, Rossjohn J, Doherty PC, Turner SJ, Kedzierska K. 2010. Protective efficacy of cross-reactive CD8$^+$ T cells recognising mutant viral epitopes depends on peptide-MHC-I structural interactions and T cell activation threshold. PLoS Pathog 6:e1001039. https://doi.org/10.1371/journal.ppat.1001039
18. Klenerman P, Zinkernagel RM. 1998. Original antigenic sin impairs cytotoxic T lymphocyte responses to viruses bearing variant epitopes. Nature 394:482–485. https://doi.org/10.1038/28860
19. Yu G, Wang LG, Han Y, He QY. 2012. clusterProfiler: an R package for comparing biological themes among gene clusters. OMICS 16:284–287. https://doi.org/10.1089/omi.2011.0118
20. van der Windt GJW, O'Sullivan D, Everts B, Huang SC-C, Buck MD, Curtis JD, Chang C-H, Smith AM, Ai T, Faubert B, Jones RG, Pearce EJ, Pearce EL. 2013. CD8 memory T cells have a bioenergetic advantage that underlies their rapid recall ability. Proc Natl Acad Sci U S A 110:14336–14341. https://doi.org/10.1073/pnas.1221740110
21. Pearce EL, Poffenberger MC, Chang CH, Jones RG. 2013. Fueling immunity: insights into metabolism and lymphocyte function. Science 342:1242454. https://doi.org/10.1126/science.1242454
22. Cortese M, Sinclair C, Pulendran B. 2014. Translating glycolytic metabolism to innate immunity in dendritic cells. Cell Metab 19:737–739. https://doi.org/10.1016/j.cmet.2014.04.012
23. Blagih J, Coulombe F, Vincent EE, Dupuy F, Galicia-Vázquez G, Yurchenko E, Raissi TC, van der Windt GJW, Viollet B, Pearce EL, Pelletier J, Piccirillo CA, Krawczyk CM, Divangahi M, Jones RG. 2015. The energy sensor AMPK regulates T cell metabolic adaptation and effector responses *in vivo*. Immunity 42:41–54. https://doi.org/10.1016/j.immuni.2014.12.030
24. Yap KL, Ada GL, McKenzie IF. 1978. Transfer of specific cytotoxic T lymphocytes protects mice inoculated with influenza virus. Nature 273:238–239. https://doi.org/10.1038/273238a0
25. Mbawuike IN, Zhang Y, Couch RB. 2007. Control of mucosal virus infection by influenza nucleoprotein-specific CD8$^+$ cytotoxic T lymphocytes. Respir Res 8:44. https://doi.org/10.1186/1465-9921-8-44
26. Taylor PM, Askonas BA. 1986. Influenza nucleoprotein-specific cytotoxic T-cell clones are protective *in vivo*. Immunology 58:417–420.
27. Christensen JP, Doherty PC, Branum KC, Riberdy JM. 2000. Profound protection against respiratory challenge with a lethal H7N7 influenza A virus by increasing the magnitude of CD8(+) T-cell memory. J Virol 74:11690–11696. https://doi.org/10.1128/jvi.74.24.11690-11696.2000
28. Sambhara S, Woods S, Arpino R, Kurichh A, Tamane A, Underdown B, Klein M, Lövgren Bengtsson K, Morein B, Burt D. 1998. Heterotypic protection against influenza by immunostimulating complexes is associated with the induction of cross-reactive cytotoxic T lymphocytes. J Infect Dis 177:1266–1274. https://doi.org/10.1086/515285
29. Sambhara S, Kurichh A, Miranda R, Tumpey T, Rowe T, Renshaw M, Arpino R, Tamane A, Kandil A, James O, Underdown B, Klein M, Katz J, Burt D. 2001. Heterosubtypic immunity against human influenza A viruses, including recently emerged avian H5 and H9 viruses, induced by FLU-ISCOM vaccine in mice requires both cytotoxic T-lymphocyte and macrophage function. Cell Immunol 211:143–153. https://doi.org/10.1006/cimm.2001.1835
30. Auladell M, Jia X, Hensen L, Chua B, Fox A, Nguyen THO, Doherty PC, Kedzierska K. 2019. Recalling the future: immunological memory toward unpredictable influenza viruses. Front Immunol 10:1400. https://doi.org/10.3389/fimmu.2019.01400
31. Moriyama M, Takeyama H, Hasegawa H, Ichinohe T. 2017. Induction of lung CD8(+) T cell responses by consecutive inoculations of a poly(I:C) influenza vaccine. Vaccine 35:6620–6626. https://doi.org/10.1016/j.vaccine.2017.10.038
32. Cargnelutti DE, Sánchez MV, Mattion NM, Scodeller EA. 2013. Development of a universal CTL-based vaccine for influenza. Bioengineered 4:374–378. https://doi.org/10.4161/bioe.23573
33. Yang J, Shim S-M, Nguyen TQ, Kim E-H, Kim K, Lim YT, Sung M-H, Webby R, Poo H. 2017. Poly-gamma-glutamic acid/chitosan nanogel greatly enhances the efficacy and heterosubtypic cross-reactivity of H1N1 pandemic influenza vaccine. Sci Rep 7:44839. https://doi.org/10.1038/srep44839
34. Herrmann VL, Hartmayer C, Planz O, Groettrup M. 2015. Cytotoxic T cell vaccination with PLGA microspheres interferes with influenza A virus replication in the lung and suppresses the infectious disease. J Control Release 216:121–131. https://doi.org/10.1016/j.jconrel.2015.08.019
35. Duan S, Thomas PG. 2016. Balancing immune protection and immune pathology by CD8(+) T-cell responses to influenza infection. Front Immunol 7:25. https://doi.org/10.3389/fimmu.2016.00025
36. Srikiatkhachorn A, Chintapalli J, Liu J, Jamaluddin M, Harrod KS, Whitsett JA, Enelow RI, Ramana CV. 2010. Interference with intraepithelial TNF-alpha signaling inhibits CD8(+) T-cell-mediated lung injury in influenza infection. Viral Immunol 23:639–645. https://doi.org/10.1089/vim.2010.0076
37. Moskophidis D, Kioussis D. 1998. Contribution of virus-specific CD8$^+$ cytotoxic T cells to virus clearance or pathologic manifestations of influenza virus infection in a T cell receptor transgenic mouse model. J Exp Med 188:223–232. https://doi.org/10.1084/jem.188.2.223
38. Mauad T, Hajjar LA, Callegari GD, da Silva LFF, Schout D, Galas FRBG, Alves VAF, Malheiros DMAC, Auler JOC Jr, Ferreira AF, Borsato MRL, Bezerra SM, Gutierrez PS, Caldini ETEG, Pasqualucci CA, Dolhnikoff M, Saldiva PHN. 2010. Lung pathology in fatal novel human influenza A (H1N1) infection. Am J Respir Crit Care Med 181:72–79. https://doi.org/10.1164/rccm.200909-1420OC
39. Kim HW, Canchola JG, Brandt CD, Pyles G, Chanock RM, Jensen K, Parrott RH. 1969. Respiratory syncytial virus disease in infants despite prior administration of antigenic inactivated vaccine. Am J Epidemiol 89:422–434. https://doi.org/10.1093/oxfordjournals.aje.a120955
40. Killikelly AM, Kanekiyo M, Graham BS. 2016. Pre-fusion F is absent on the surface of formalin-inactivated respiratory syncytial virus. Sci Rep 6:34108. https://doi.org/10.1038/srep34108
41. Sabbaghi A, Miri SM, Keshavarz M, Zargar M, Ghaemi A. 2019. Inactivation methods for whole influenza vaccine production. Rev Med Virol 29:e2074. https://doi.org/10.1002/rmv.2074
42. Fan Y-C, Chiu H-C, Chen L-K, Chang G-JJ, Chiou S-S. 2015. Formalin inactivation of Japanese encephalitis virus vaccine alters the antigenicity

and immunogenicity of a neutralization epitope in envelope protein domain III. PLoS Negl Trop Dis 9:e0004167. https://doi.org/10.1371/journal.pntd.0004167
43. Tumpey TM, Renshaw M, Clements JD, Katz JM. 2001. Mucosal delivery of inactivated influenza vaccine induces B-cell-dependent heterosubtypic cross-protection against lethal influenza A H5N1 virus infection. J Virol 75:5141–5150. https://doi.org/10.1128/JVI.75.11.5141-5150.2001
44. Curtsinger JM, Mescher MF. 2010. Inflammatory cytokines as a third signal for T cell activation. Curr Opin Immunol 22:333–340. https://doi.org/10.1016/j.coi.2010.02.013
45. Pfistershammer K, Majdic O, Stöckl J, Zlabinger G, Kirchberger S, Steinberger P, Knapp W. 2004. CD63 as an activation-linked T cell costimulatory element. J Immunol 173:6000–6008. https://doi.org/10.4049/jimmunol.173.10.6000
46. Thomas IJ, Petrich de Marquesini LG, Ravanan R, Smith RM, Guerder S, Flavell RA, Wraith DC, Wen L, Wong FS. 2007. CD86 has sustained costimulatory effects on CD8 T cells. J Immunol 179:5936–5946. https://doi.org/10.4049/jimmunol.179.9.5936
47. Witherden DA, Boismenu R, Havran WL. 2000. CD81 and CD28 costimulate T cells through distinct pathways. J Immunol 165:1902–1909. https://doi.org/10.4049/jimmunol.165.4.1902
48. Peeters MJW, Dulkeviciute D, Draghi A, Ritter C, Rahbech A, Skadborg SK, Seremet T, Carnaz Simões AM, Martinenaite E, Halldórsdóttir HR, Andersen MH, Olofsson GH, Svane IM, Rasmussen LJ, Met Ö, Becker JC, Donia M, Desler C, thor Straten P. 2019. MERTK acts as a costimulatory receptor on human CD8(+) T cells. Cancer Immunol Res 7:1472–1484. https://doi.org/10.1158/2326-6066.CIR-18-0841
49. Arneth B. 2015. Early activation of $CD4^+$ and $CD8^+$ T lymphocytes by myelin basic protein in subjects with MS. J Transl Med 13:341. https://doi.org/10.1186/s12967-015-0715-6
50. Correia MP, Costa AV, Uhrberg M, Cardoso EM, Arosa FA. 2011. IL-15 induces $CD8^+$ T cells to acquire functional NK receptors capable of modulating cytotoxicity and cytokine secretion. Immunobiology 216:604–612. https://doi.org/10.1016/j.imbio.2010.09.012
51. Mohammed RN, Wehenkel SC, Galkina EV, Yates E-K, Preece G, Newman A, Watson HA, Ohme J, Bridgeman JS, Durairaj RRP, Moon OR, Ladell K, Miners KL, Dolton G, Troeberg L, Kashiwagi M, Murphy G, Nagase H, Price DA, Matthews RJ, Knäuper V, Ager A. 2019. ADAM17-dependent proteolysis of L-selectin promotes early clonal expansion of cytotoxic T cells. Sci Rep 9:5487. https://doi.org/10.1038/s41598-019-41811-z
52. Ngo Thai Bich V, Hongu T, Miura Y, Katagiri N, Ohbayashi N, Yamashita-Kanemaru Y, Shibuya A, Funakoshi Y, Kanaho Y. 2018. Physiological function of phospholipase D2 in anti-tumor immunity: regulation of CD8(+) T lymphocyte proliferation. Sci Rep 8:6283. https://doi.org/10.1038/s41598-018-24512-x
53. Sarkar S, Yuzefpolskiy Y, Xiao H, Baumann FM, Yim S, Lee DJ, Schenten D, Kalia V. 2018. Programming of CD8 T cell quantity and polyfunctionality by direct IL-1 signals. J Immunol 201:3641–3650. https://doi.org/10.4049/jimmunol.1800906
54. Zhang N, Bevan MJ. 2011. CD8(+) T cells: foot soldiers of the immune system. Immunity 35:161–168. https://doi.org/10.1016/j.immuni.2011.07.010
55. Li Y, Tang L, Guo L, Chen C, Gu S, Zhou Y, Ye G, Li X, Wang W, Liao X, Wang Y, Peng X, Liu G, Zhang X, Sun J, Peng J, Hou J. 2020. CXCL13-mediated recruitment of intrahepatic CXCR5(+)CD8(+) T cells favors viral control in chronic HBV infection. J Hepatol 72:420–430. https://doi.org/10.1016/j.jhep.2019.09.031
56. Lee LN, Baban D, Ronan EO, Ragoussis J, Beverley PCL, Tchilian EZ. 2010. Chemokine gene expression in lung CD8 T cells correlates with protective immunity in mice immunized intra-nasally with Adenovirus-85A. BMC Med Genomics 3:46. https://doi.org/10.1186/1755-8794-3-46
57. Paterson S, Kar S, Ung SK, Gardener Z, Bergstrom E, Ascough S, Kalyan M, Zyla J, Maertzdorf J, Mollenkopf H-J, Weiner J, Jozwik A, Jarvis H, Jha A, Nicholson BP, Veldman T, Woods CW, Mallia P, Kon OM, Kaufmann SHE, Openshaw PJ, Chiu C. 2021. Innate-like gene expression of lung-resident memory CD8(+) T cells during experimental human influenza: a clinical study. Am J Respir Crit Care Med 204:826–841. https://doi.org/10.1164/rccm.202103-0620OC
58. Guo Y, Lee YC, Brown C, Zhang W, Usherwood E, Noelle RJ. 2014. Dissecting the role of retinoic acid receptor isoforms in the CD8 response to infection. J Immunol 192:3336–3344. https://doi.org/10.4049/jimmunol.1301949
59. Poczobutt JM, Nguyen TT, Hanson D, Li H, Sippel TR, Weiser-Evans MCM, Gijon M, Murphy RC, Nemenoff RA. 2016. Deletion of 5-lipoxygenase in the tumor microenvironment promotes lung cancer progression and metastasis through regulating T cell recruitment. J Immunol 196:891–901. https://doi.org/10.4049/jimmunol.1501648
60. Nishimura M, Umehara H, Nakayama T, Yoneda O, Hieshima K, Kakizaki M, Dohmae N, Yoshie O, Imai T. 2002. Dual functions of fractalkine/CX3C ligand 1 in trafficking of perforin+/granzyme B+ cytotoxic effector lymphocytes that are defined by CX3CR1 expression. J Immunol 168:6173–6180. https://doi.org/10.4049/jimmunol.168.12.6173
61. Mensali N, Grenov A, Pati NB, Dillard P, Myhre MR, Gaudernack G, Kvalheim G, Inderberg EM, Bakke O, Wälchli S. 2019. Antigen-delivery through invariant chain (CD74) boosts CD8 and CD4 T cell immunity. Oncoimmunology 8:1558663. https://doi.org/10.1080/2162402X.2018.1558663
62. Diaz LS, Foster H, Stone MR, Fujimura S, Relman DA, Levy JA. 2005. VCAM-1 expression on $CD8^+$ cells correlates with enhanced anti-HIV suppressing activity. J Immunol 174:1574–1579. https://doi.org/10.4049/jimmunol.174.3.1574
63. Borger JG, Morrison VL, Filby A, Garcia C, Uotila LM, Simbari F, Fagerholm SC, Zamoyska R. 2017. Caveolin-1 influences LFA-1 redistribution upon TCR stimulation in CD8 T cells. J Immunol 199:874–884. https://doi.org/10.4049/jimmunol.1700431
64. Ma JSY, Haydar TF, Radoja S. 2008. Protein kinase C delta localizes to secretory lysosomes in $CD8^+$ CTL and directly mediates TCR signals leading to granule exocytosis-mediated cytotoxicity. J Immunol 181:4716–4722. https://doi.org/10.4049/jimmunol.181.7.4716
65. Gao L, Wang Y, Li Y, Dong Y, Yang A, Zhang 3,J, Li 5,F, Zhang R. 2018. Genome-wide expression profiling analysis to identify key genes in the anti-HIV mechanism of CD4(+) and CD8(+) T cells. J Med Virol 90:1199–1209. https://doi.org/10.1002/jmv.25071
66. Yeung T-L, Tsai CC, Leung CS, Au Yeung C-L, Thompson MS, Lu KH, Freedman RS, Birrer MJ, Wong K-K, Mok SC. 2018. ISG15 promotes ERK1 ISGylation, $CD8^+$ T cell activation and suppresses ovarian cancer progression. Cancers (Basel) 10:12. https://doi.org/10.3390/cancers10120464
67. Zhou A, Dong X, Liu M, Tang B. 2021. Comprehensive transcriptomic analysis identifies novel antiviral factors against influenza A virus infection. Front Immunol 12:632798. https://doi.org/10.3389/fimmu.2021.632798
68. Boon ACM, de Mutsert G, Fouchier RAM, Osterhaus ADME, Rimmelzwaan GF. 2005. Functional profile of human influenza virus-specific cytotoxic T lymphocyte activity is influenced by interleukin-2 concentration and epitope specificity. Clin Exp Immunol 142:45–52. https://doi.org/10.1111/j.1365-2249.2005.02880.x
69. Chang C-H, Curtis JD, Maggi LB Jr, Faubert B, Villarino AV, O'Sullivan D, Huang SC-C, van der Windt GJW, Blagih J, Qiu J, Weber JD, Pearce EJ, Jones RG, Pearce EL. 2013. Posttranscriptional control of T cell effector function by aerobic glycolysis. Cell 153:1239–1251. https://doi.org/10.1016/j.cell.2013.05.016
70. Pearce EL, Pearce EJ. 2013. Metabolic pathways in immune cell activation and quiescence. Immunity 38:633–643. https://doi.org/10.1016/j.immuni.2013.04.005
71. Buck MD, O'Sullivan D, Klein Geltink RI, Curtis JD, Chang C-H, Sanin DE, Qiu J, Kretz O, Braas D, van der Windt GJW, Chen Q, Huang SC-C, O'Neill CM, Edelson BT, Pearce EJ, Sesaki H, Huber TB, Rambold AS, Pearce EL. 2016. Mitochondrial dynamics controls T cell fate through metabolic programming. Cell 166:63–76. https://doi.org/10.1016/j.cell.2016.05.035
72. Pearce EL. 2021. Metabolism as a driver of immunity. Nat Rev Immunol 21:618–619. https://doi.org/10.1038/s41577-021-00601-3
73. Hillaire MLB, van Trierum SE, Kreijtz JHCM, Bodewes R, Geelhoed-Mieras MM, Nieuwkoop NJ, Fouchier RAM, Kuiken T, Osterhaus ADME, Rimmelzwaan GF. 2011. Cross-protective immunity against influenza pH1N1 2009 viruses induced by seasonal influenza A (H3N2) virus is mediated by virus-specific T-cells. J Gen Virol 92:2339–2349. https://doi.org/10.1099/vir.0.033076-0
74. Jameson J, Cruz J, Ennis FA. 1998. Human cytotoxic T-lymphocyte repertoire to influenza A viruses. J Virol 72:8682–8689. https://doi.org/10.1128/JVI.72.11.8682-8689.1998

75. Cao W, Liepkalns JS, Hassan AO, Kamal RP, Hofstetter AR, Amoah S, Kim JH, Reber AJ, Stevens J, Katz JM, Gangappa S, York IA, Mittal SK, Sambhara S. 2016. A highly immunogenic vaccine against A/H7N9 influenza virus. Vaccine 34:744–749. https://doi.org/10.1016/j.vaccine.2015.12.062
76. Pandey A, Singh N, Vemula SV, Couëtil L, Katz JM, Donis R, Sambhara S, Mittal SK. 2012. Impact of preexisting adenovirus vector immunity on immunogenicity and protection conferred with an adenovirus-based H5N1 influenza vaccine. PLoS One 7:e33428. https://doi.org/10.1371/journal.pone.0033428
77. van Olphen AL, Mittal SK. 2002. Development and characterization of bovine x human hybrid cell lines that efficiently support the replication of both wild-type bovine and human adenoviruses and those with E1 deleted. J Virol 76:5882–5892. https://doi.org/10.1128/jvi.76.12.5882-5892.2002
78. Bray NL, Pimentel H, Melsted P, Pachter L. 2016. Near-optimal probabilistic RNA-seq quantification. Nat Biotechnol 34:525–527. https://doi.org/10.1038/nbt.3519
79. Soneson C, Love MI, Robinson MD. 2015. Differential analyses for RNA-seq: transcript-level estimates improve gene-level inferences. F1000Res 4:1521. https://doi.org/10.12688/f1000research.7563.2
80. Hardcastle TJ, Kelly KA. 2010. baySeq: empirical Bayesian methods for identifying differential expression in sequence count data. BMC Bioinformatics 11:422. https://doi.org/10.1186/1471-2105-11-422
81. Robinson MD, McCarthy DJ, Smyth GK. 2010. edgeR: a Bioconductor package for differential expression analysis of digital gene expression data. Bioinformatics 26:139–140. https://doi.org/10.1093/bioinformatics/btp616
82. Love MI, Huber W, Anders S. 2014. Moderated estimation of fold change and dispersion for RNA-seq data with DESeq2. Genome Biol 15:550. https://doi.org/10.1186/s13059-014-0550-8
83. Wickham H. 2016. ggplot2: elegant graphics for data analysis (use R). 2nd ed. Springer, Cham.
84. Gu Z, Eils R, Schlesner M. 2016. Complex heatmaps reveal patterns and correlations in multidimensional genomic data. Bioinformatics 32:2847–2849. https://doi.org/10.1093/bioinformatics/btw313